

Invariant mass distributions in cascade decays

D. J. Miller

Department of Physics and Astronomy, University of Glasgow, Glasgow G12 8QQ, U.K.

E-mail: D.Miller@physics.gla.ac.uk

P. Osland

Department of Physics, University of Bergen, N-5007 Bergen, Norway

and TH Division, Physics Department, CERN, CH 1211 Genève, Switzerland

E-mail: Per.Osland@ift.uib.no

A. R. Raklev

Department of Physics, University of Bergen, N-5007 Bergen, Norway

and TH Division, Physics Department, CERN, CH 1211 Genève, Switzerland

E-mail: Are.Raklev@ift.uib.no

ABSTRACT: We derive analytical expressions for the shape of the invariant mass distributions of massless Standard Model endproducts in cascade decays involving massive New Physics (NP) particles, $D \rightarrow Cc \rightarrow Bbc \rightarrow Aabc$, where the final NP particle A in the cascade is unobserved and where two of the particles a, b, c may be indistinguishable. Knowledge of these expressions can improve the determination of NP parameters at the LHC. The shape formulas are composite, but contain nothing more complicated than logarithms of simple expressions. We study the effects of cuts, final state radiation and detector effects on the distributions through Monte Carlo simulations, using a supersymmetric model as an example. We also consider how one can deal with the width of NP particles and with combinatorics from the misidentification of final state particles. The possible mismeasurements of NP masses through “feet” in the distributions are discussed. Finally, we demonstrate how the effects of different spin configurations can be included in the distributions.

KEYWORDS: SUSY, BSM, MSSM.

Contents

1. Introduction	2
2. Invariant mass distributions	3
2.1 The two-particle invariant mass m_{ca}	4
2.2 The two-particle invariant mass $m_{c2(\text{high})}$	7
2.2.1 Region 1: $\frac{1}{2-R_A} < R_B < 1$	9
2.2.2 Region 2: $R_A < R_B < \frac{1}{2-R_A}$	10
2.2.3 Region 3: $0 < R_B < R_A$	11
2.3 The two-particle invariant mass $m_{c2(\text{low})}$	12
2.3.1 Region 1: $\frac{1}{2-R_A} < R_B < 1$	13
2.3.2 Regions 2 and 3: $0 < R_B < \frac{1}{2-R_A}$	13
2.4 The three-particle invariant mass m_{cba}	14
2.4.1 Region 1: $0 < R_C < R_A R_B < 1$	18
2.4.2 Region 2: $0 < \frac{R_B}{R_A} < R_C < 1$	19
2.4.3 Region 3: $0 < \frac{R_A}{R_B} < R_C < 1$	19
2.4.4 Region 4: $0 < R_A R_B < R_C$ and $R_C < \frac{R_B}{R_A} < 1$ and $R_C < \frac{R_A}{R_B} < 1$	19
3. Parton level	20
3.1 Width	21
3.2 Cuts	21
3.3 Final state radiation	23
4. Detector effects	24
5. Feet	27
5.1 $m_{c2(\text{high})}$	28
5.2 $m_{c2(\text{low})}$	28
5.3 m_{cba}	29
5.4 SPS benchmark points	30
6. Summary	31
A. Including spin in a SUSY scenario	33
A.1 m_{ca}	34
A.2 $m_{c2(\text{high})}$	35
A.3 $m_{c2(\text{low})}$	36
A.4 m_{cba}	36

1. Introduction

While the discovery of a broken TeV-scale supersymmetry [1, 2, 3, 4, 5] at the LHC would solve many problems in modern particle physics, it would also raise many questions. For example, do the forces unify at some high scale, as the supersymmetric evolution of couplings imply; what is the mechanism of supersymmetry breaking; does supersymmetry provide a viable dark matter candidate? To answer any of these questions it is important to have accurate measurements of the supersymmetric partner masses.

In the Minimal Supersymmetric Standard Model (MSSM), superpartner production cross-sections at the LHC are rather large, allowing the discovery of squarks and gluinos with masses up to about 2.5 TeV. Nevertheless, if R-parity is conserved, the traditional method of measuring masses from resonant peaks in invariant mass distributions cannot be easily used for superpartners. The end products of every superpartner decay necessarily include the lightest supersymmetric particle (LSP) which is stable and escapes the detector, preventing full reconstruction. However, invariant mass distributions constructed from the *visible* particles in a decay chain clearly do depend on the masses of their parents, and it should be possible to extract these masses in a systematic way. In particular, the kinematic endpoints of these invariant mass distributions (i.e. their minimum or maximum values) can be measured and their relation to the unknown superpartner masses can be exploited. This method has been widely studied in refs. [6, 7, 8, 9, 10, 11, 12, 13].

This study builds upon the work of ref. [12] which investigated the measurement of superpartner masses via the endpoint method for the decay¹

$$\tilde{q}_L \rightarrow \tilde{\chi}_2^0 q \rightarrow \tilde{l}_R l_n q \rightarrow \tilde{\chi}_1^0 l_f l_n q \quad (1.1)$$

at the Snowmass mSUGRA benchmark point SPS 1a [14]. Several problems with the endpoint method were uncovered. These include the possibility of multiple minima in global least squares fits to the masses and mismeasurements of the endpoints due to the occurrence of “feet” in the distributions.

Supersymmetry is not the only New Physics (NP) scenario that can be discovered at the LHC and which gives rise to long decay chains. In universal extra dimension models (UED) [15], Kaluza-Klein (KK) excitations of Standard Model (SM) particles could have experimental signatures very similar to SUSY models. In [16] the possibility of the decay chain

$$Q_1 \rightarrow Z_1 q \rightarrow L_1 l_n q \rightarrow \gamma_1 l_f l_n q \quad (1.2)$$

was pointed out. Here the subscript 1 denotes the first KK-excitations of the SM particles. Indeed the occurrence of a similar decay chain in any multi-particle NP model which has a good dark matter candidate should not be a surprise. The dark matter candidate should be a weakly interacting, neutral and massive particle, thus escaping the detector. This particle must be kept stable by some symmetry, in our examples R-parity for SUSY and KK-parity for UED, and this symmetry is likely also to conserve the number of NP particles in decays, creating a decay cascade through the hierarchy of NP masses.

¹The subscripts n and f on the leptons, representing “near” and “far”, denote the first and second lepton emitted in the decay.

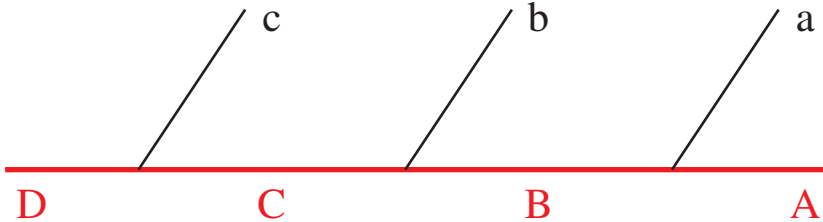


Figure 1: Decay chain. Particles c , b and a are assumed massless.

In light of this we will maintain a degree of generality in our derivation. We derive analytic formulae for the invariant mass distributions of particles in the decay chain

$$D \rightarrow Cc \rightarrow Bbc \rightarrow Aabc, \quad (1.3)$$

illustrated in figure 1, where D , C , B and A are massive, satisfying

$$m_D > m_C > m_B > m_A, \quad (1.4)$$

and the particles a , b , c are taken to be massless.

With A invisible, we can form four invariant mass combinations of the decay products c , b and a : m_{ba} , m_{cb} , m_{ca} and m_{cba} . However, both the decay chains (1.1) and (1.2) give two opposite sign, same flavour leptons, l_n and l_f , which are in principle indistinguishable. This is a general feature of decay chains; given a SM decay product with a particular flavour this flavour should be carried on in the decay chain and may result in two same flavour decay products. We will deal with this by calculating the shape of the distributions of the invariant masses $m_{c2(\text{low})}$ and $m_{c2(\text{high})}$, which are the invariant masses of c combined with either b or a , depending on which gives the lower and higher invariant mass.

In the following section we derive the shapes of these invariant mass distributions. Using the decay chain (1.1) as an example we consider in section 3 some complicating effects present already at the parton level, such as final state radiation, cuts and the width of the SUSY particles. In section 4 we further look at detector induced effects on the distributions and in section 5 we discuss a possible application of the shapes of the invariant masses to alleviate the problem with “feet”. In section 6 we give a brief summary of our results. The inclusion of spin effects is discussed in an appendix. An application of the shape formulas to Monte Carlo data for the purposes of improving mass determination at the LHC will be presented elsewhere.

2. Invariant mass distributions

Our aim here is to obtain expressions for the invariant mass distributions of cascade decays such as (1.3), which can be compared to data to fit NP particle masses. These distributions can be easily calculated numerically by Monte Carlo integration, and indeed we use

the Monte Carlo event generator PYTHIA [17] to numerically check our analytic results. However, Monte Carlo integration (via phase space generation) is slow in comparison to the evaluation of an analytic expression, which makes it impractical for fitting masses, or performing other comparisons, where many distributions for different masses must be generated. For this reason we derive analytic expressions.

In the main part of the paper, we will assume that there are no spin correlations between the subsequent decays, and thus treat the decaying particles as if they were scalars (see, however, the appendix). Indeed, PYTHIA 6.208 uses this simplification in its generation of phase space. This has been shown to be a reasonable simplification for the decay chains of physical interest as long as one does not measure the charges of the final state particles [18, 19], which for jets would be very difficult to do. However, it has been suggested in [19, 20] that measurements of NP particle spin is possible at the LHC because of the asymmetry between produced squarks and antisquarks. The method used in the derivation of the invariant mass distributions can fairly easily be adapted to a particular spin configuration of the particles in the decay chain and distributions including spin effects are given in the appendix for our SUSY example. For simplicity of the analytic expressions, we will also ignore particle widths. The effects of widths can be added later by a smearing of the distributions.

Our philosophy for calculating the invariant mass distributions will be to write the square of the invariant masses in terms of angular variables in the rest frame of decaying particles. In the spin-0 case these have isotropic, flat distributions. After performing a transformation from these ‘flat’ variables to a set of variables which include the invariant mass under discussion, an integration over the extra variables can be performed to provide the desired distribution. The difficulty of the calculation will be seen not to lie in performing the integrals, but in finding the correct integration interval for all possible configurations of masses that obey eq. (1.4). Spin effects only complicate the integrand and not the endpoints of the integration.

Distributions formed from two “neighbouring” particles, m_{cb} and m_{ba} , have simple triangular shapes when widths and spin are ignored (see e.g. figure 10 and eq. (4.2) of [12]), and will not be discussed further here. We will also limit our discussion to cases where the intermediate NP particles C and B are on-shell. For a discussion on the shape of distributions in the SUSY scenario of eq. (1.1), with virtual particles in the decay chain, see [21].

2.1 The two-particle invariant mass m_{ca}

The invariant mass m_{ca} is given by

$$m_{ca}^2 \equiv (p_c + p_a)^2 = 2E_c^{(B)} E_a^{(B)} \left(1 - \cos \theta_{ca}^{(B)}\right), \quad (2.1)$$

where $E_a^{(B)}$ and $E_c^{(B)}$ are the energies of a and c respectively and $\theta_{ca}^{(B)}$ is the angle between c and a , all in the rest frame of B , denoted by the superscript (B) . Energy and momentum conservation in the decays of the B , C and D additionally provide

$$E_a^{(B)} = \frac{m_B^2 - m_A^2}{2m_B}, \quad (2.2)$$

$$E_b^{(B)} = \frac{m_C^2 - m_B^2}{2m_B}, \quad (2.3)$$

$$E_c^{(B)} = \frac{(m_D^2 - m_C^2) m_B}{(m_C^2 + m_B^2) - (m_C^2 - m_B^2) \cos \theta_{cb}^{(B)}}, \quad (2.4)$$

where $\theta_{cb}^{(B)}$ is the angle between c and b in (B) . It will be convenient to introduce three further quantities,

$$(m_{ca}^{\max})^2 = \frac{(m_D^2 - m_C^2) (m_B^2 - m_A^2)}{m_B^2}, \quad (2.5)$$

$$(m_{cb}^{\max})^2 = \frac{(m_D^2 - m_C^2) (m_C^2 - m_B^2)}{m_C^2}, \quad (2.6)$$

$$(m_{c2(\text{eq})}^{\max})^2 = \frac{(m_D^2 - m_C^2) (m_B^2 - m_A^2)}{2m_B^2 - m_A^2}, \quad (2.7)$$

where m_{ca}^{\max} and m_{cb}^{\max} are the maximum possible values of m_{ca} and m_{cb} respectively, while $m_{c2(\text{eq})}$ is a possible maximum of the $m_{c2(\text{low})}$ distribution (see sect. 2.3).

From the above, it follows that

$$m_{ca}^2 = (m_{ca}^{\max})^2 \frac{m_B^2 (1 - \cos \theta_{ca}^{(B)})}{(m_C^2 + m_B^2) - (m_C^2 - m_B^2) \cos \theta_{cb}^{(B)}}. \quad (2.8)$$

Following our philosophy of writing the invariant mass in terms of variables with flat distributions we now express $\cos \theta_{cb}^{(B)}$ in terms of $\cos \theta_{cb}^{(C)}$, the same angle in the rest frame of C . If C is a scalar this angle will be isotropically distributed. If C is *not* a scalar, the angular distribution will depend on the helicities of b and c . However, summing over particles and antiparticles in the final state will cancel these spin correlations and return an isotropic distribution. This latter case is applicable here.

In the rest frame of C we have the familiar result

$$m_{cb}^2 = (m_{cb}^{\max})^2 \left(\frac{1 - \cos \theta_{cb}^{(C)}}{2} \right). \quad (2.9)$$

Using eqs. (2.3) and (2.4), the same invariant mass in (B) is given by

$$m_{cb}^2 = (m_{cb}^{\max})^2 \frac{m_C^2 (1 - \cos \theta_{cb}^{(B)})}{(m_C^2 + m_B^2) - (m_C^2 - m_B^2) \cos \theta_{cb}^{(B)}}. \quad (2.10)$$

Equating the two expressions and solving for $1 - \cos \theta_{cb}^{(B)}$ gives

$$1 - \cos \theta_{cb}^{(B)} = 2 \left[1 + \frac{m_C^2}{m_B^2} \frac{1 + \cos \theta_{cb}^{(C)}}{1 - \cos \theta_{cb}^{(C)}} \right]^{-1}, \quad (2.11)$$

and consequently

$$m_{ca}^2 = (m_{ca}^{\max})^2 \left[\frac{m_B^2}{m_C^2} \left(\frac{1 - \cos \theta_{cb}^{(C)}}{2} \right) + \left(\frac{1 + \cos \theta_{cb}^{(C)}}{2} \right) \right] \left(\frac{1 - \cos \theta_{ca}^{(B)}}{2} \right). \quad (2.12)$$

We have now written the invariant mass in terms of quantities which have isotropic distributions. Adopting the notation

$$u \equiv \frac{1 - \cos \theta_{cb}^{(C)}}{2}, \quad v \equiv \frac{1 - \cos \theta_{ca}^{(B)}}{2} \quad (2.13)$$

we observe that the differential decay widths for these observables are flat for $0 \leq (u, v) \leq 1$:

$$\frac{1}{\Gamma_0} \frac{\partial^2 \Gamma_0}{\partial u \partial v} = \theta(1-u)\theta(u)\theta(1-v)\theta(v), \quad (2.14)$$

where $\theta(x)$ is the usual step function, and where the subscript “0” is a reminder that spin correlations are omitted (however, see the Appendix). We can now make a change of variables from (u, v) to (u, m_{ca}^2) with

$$m_{ca}^2 = (m_{ca}^{\max})^2 (1 - au) v, \quad (2.15)$$

where, for abbreviation of the equations to follow, we have written

$$a \equiv 1 - \frac{m_B^2}{m_C^2}, \quad 0 < a < 1. \quad (2.16)$$

This gives the differential distribution

$$\begin{aligned} \frac{1}{\Gamma_0} \frac{\partial^2 \Gamma_0}{\partial u \partial m_{ca}^2} &= \left| \frac{\partial(u, v)}{\partial(u, m_{ca}^2)} \right| \theta(1-u)\theta(u)\theta(1-v)\theta(v) \\ &= \hat{\theta} \left(\frac{m_{ca}^2}{(m_{ca}^{\max})^2 (1 - au)} \right) \frac{\hat{\theta}(u)}{(m_{ca}^{\max})^2 (1 - au)}, \end{aligned} \quad (2.17)$$

where for ease of notation we have defined a “top-hat” function $\hat{\theta}(x) \equiv \theta(x)\theta(1-x)$. Finally we must now integrate over u to find the distribution of m_{ca}^2 :

$$\begin{aligned} \frac{1}{\Gamma_0} \frac{\partial \Gamma_0}{\partial m_{ca}^2} &= \int_{-\infty}^{\infty} \frac{1}{\Gamma_0} \frac{\partial^2 \Gamma_0}{\partial u \partial m_{ca}^2} du \\ &= \int_0^1 \hat{\theta} \left(\frac{m_{ca}^2}{(m_{ca}^{\max})^2 (1 - au)} \right) \frac{1}{(m_{ca}^{\max})^2 (1 - au)} du \\ &= \int_0^{u_{\max}} \frac{1}{(m_{ca}^{\max})^2 (1 - au)} du \end{aligned} \quad (2.18)$$

for $0 \leq m_{ca} \leq m_{ca}^{\max}$, where

$$u_{\max} = \min \left(1, \frac{1}{a} \left[1 - \frac{m_{ca}^2}{(m_{ca}^{\max})^2} \right] \right). \quad (2.19)$$

Evaluating the integrals we find

$$\frac{1}{\Gamma_0} \frac{\partial \Gamma_0}{\partial m_{ca}^2} = \begin{cases} \frac{1}{(m_{ca}^{\max})^2 a} \ln \frac{m_C^2}{m_B^2} & \text{for } 0 < m_{ca} < \frac{m_B}{m_C} m_{ca}^{\max}, \\ \frac{1}{(m_{ca}^{\max})^2 a} \ln \frac{(m_{ca}^{\max})^2}{m_{ca}^2} & \text{for } \frac{m_B}{m_C} m_{ca}^{\max} < m_{ca} < m_{ca}^{\max}, \end{cases} \quad (2.20)$$

and zero otherwise.

From the distribution of the square of an invariant mass m^2 , it is a trivial task to find the distribution of the invariant mass as

$$\frac{1}{\Gamma_0} \frac{\partial \Gamma_0}{\partial m} = 2m \frac{1}{\Gamma_0} \frac{\partial \Gamma_0}{\partial m^2}. \quad (2.21)$$

2.2 The two-particle invariant mass $m_{c2(\text{high})}$

Having demonstrated the basic method for the simplest non-trivial case, we now turn to the more complicated problem of finding the distribution of the observable quantity $m_{c2(\text{high})}$, defined by

$$m_{c2(\text{high})} \equiv \max(m_{cb}, m_{ca}). \quad (2.22)$$

Here, m_{cb}^2 and m_{ca}^2 are given by eqs. (2.9) and (2.15), respectively. In the notation of eq. (2.13), the required invariant mass squared can be written as

$$m_{c2(\text{high})}^2 = \max[(m_{cb}^{\max})^2 u, (m_{ca}^{\max})^2 (1 - au)v]. \quad (2.23)$$

We now introduce a new variable,

$$x = (m_{cb}^{\max})^2 u - (m_{ca}^{\max})^2 (1 - au)v, \quad (2.24)$$

so that the sign of x picks out which of m_{cb} or m_{ca} is larger. Then

$$m_{c2(\text{high})}^2 = \theta(x)(m_{cb}^{\max})^2 u + \theta(-x)(m_{ca}^{\max})^2 (1 - au)v.$$

The new variables can be inverted to give

$$u = \frac{m_{c2(\text{high})}^2 + \theta(-x)x}{(m_{cb}^{\max})^2}, \quad v = \frac{m_{c2(\text{high})}^2 - \theta(x)x}{(m_{ca}^{\max})^2 \left(1 - a \frac{m_{c2(\text{high})}^2 + \theta(-x)x}{(m_{cb}^{\max})^2}\right)}. \quad (2.25)$$

Since the double-differential width with respect to u and v is flat [see eq. (2.14)], we may write

$$\begin{aligned} \frac{1}{\Gamma_0} \frac{\partial^2 \Gamma_0}{\partial x \partial m_{c2(\text{high})}^2} &= \left| \frac{\partial(u, v)}{\partial(x, m_{c2(\text{high})}^2)} \right| \hat{\theta}(u) \hat{\theta}(v) \\ &= \frac{\hat{\theta}(u) \hat{\theta}(v)}{(m_{ca}^{\max})^2 (m_{cb}^{\max})^2 (1 - au)}, \end{aligned} \quad (2.26)$$

and integrate over x to give the desired distribution:

$$\frac{1}{\Gamma_0} \frac{\partial \Gamma_0}{\partial m_{c2(\text{high})}^2} = \int_0^\infty \hat{\theta}(u_+) \hat{\theta}(v_+) \frac{1}{(m_{ca}^{\max})^2 (m_{cb}^{\max})^2 (1 - au_+)} dx$$

$$+ \int_{-\infty}^0 \hat{\theta}(u_-) \hat{\theta}(v_-) \frac{1}{(m_{ca}^{\max})^2 (m_{cb}^{\max})^2 (1 - au_-)} dx. \quad (2.27)$$

In the above we have written u_{\pm} and v_{\pm} for u and v in the case of positive/negative x , i.e.,

$$u_- = \frac{m_{c2(\text{high})}^2 + x}{(m_{cb}^{\max})^2}, \quad u_+ = \frac{m_{c2(\text{high})}^2}{(m_{cb}^{\max})^2}, \quad (2.28)$$

$$v_- = \frac{m_{c2(\text{high})}^2}{(m_{ca}^{\max})^2 \left(1 - a \frac{m_{c2(\text{high})}^2 + x}{(m_{cb}^{\max})^2}\right)}, \quad v_+ = \frac{m_{c2(\text{high})}^2 - x}{(m_{ca}^{\max})^2 \left(1 - a \frac{m_{c2(\text{high})}^2}{(m_{cb}^{\max})^2}\right)}. \quad (2.29)$$

While the integrals themselves are trivial, we must take special care with the integration endpoints. The step-functions restrict $0 < u_{\pm} < 1$ and $0 < v_{\pm} < 1$, which in turn give restrictions on x and/or $m_{c2(\text{high})}$:

$$\hat{\theta}(u_+) \neq 0 \Rightarrow \quad 0 < m_{c2(\text{high})} < m_{cb}^{\max}, \quad (2.30)$$

$$\hat{\theta}(v_+) \neq 0 \Rightarrow \quad \left[\frac{a(m_{ca}^{\max})^2}{(m_{cb}^{\max})^2} + 1 \right] m_{c2(\text{high})}^2 - (m_{ca}^{\max})^2 < x < m_{c2(\text{high})}^2, \quad (2.31)$$

$$\hat{\theta}(u_-) \neq 0 \Rightarrow \quad -m_{c2(\text{high})}^2 < x < (m_{cb}^{\max})^2 - m_{c2(\text{high})}^2, \quad (2.32)$$

$$\hat{\theta}(v_-) \neq 0 \Rightarrow \quad x < \frac{(m_{cb}^{\max})^2}{a} - \left[\frac{(m_{cb}^{\max})^2}{a(m_{ca}^{\max})^2} + 1 \right] m_{c2(\text{high})}^2. \quad (2.33)$$

The first two inequalities constrain the integration over positive values of x , while the last two constrain the integration over negative values of x . Notice that v_- only provides one inequality since the condition $\theta(v_-) \neq 0$ holds when (2.32) holds. Also $\theta(v_+) \neq 0$ yields an upper bound on x because the denominator of v_+ is always positive when (2.30) holds.

Which of these inequalities provides the strongest bound and thereby the endpoint of the integration is highly dependent on the mass hierarchy between particles A , B and C . In particular, the various bounds on x coincide at four (non-trivial) distinct values of $m_{c2(\text{high})}$, namely m_{ca}^{\max} , m_{cb}^{\max} , $\frac{m_B}{m_C} m_{ca}^{\max}$ and $m_{c2(\text{eq})}^{\max}$, and it is the relative size of these four quantities which is important. With this in mind we define three different regions, exhausting all possible hierarchies. Writing

$$R_A \equiv \frac{m_A^2}{m_B^2}, \quad R_B \equiv \frac{m_B^2}{m_C^2}, \quad R_C \equiv \frac{m_C^2}{m_D^2}, \quad (2.34)$$

(R_C is defined for later reference), the different mass hierarchies can be divided into:

$$\begin{aligned} \text{Region 1:} & \quad \frac{1}{2-R_A} < R_B < 1, \\ \text{Region 2:} & \quad R_A < R_B < \frac{1}{2-R_A}, \\ \text{Region 3:} & \quad 0 < R_B < R_A. \end{aligned}$$

The three regions are shown in figure 2 over the space of R_A and R_B .

2.2.1 Region 1: $\frac{1}{2-R_A} < R_B < 1$

In Region 1, we have

$$m_{cb}^{\max} < m_{c2(\text{eq})}^{\max} < \frac{m_B}{m_C} m_{ca}^{\max} < m_{ca}^{\max}. \quad (2.35)$$

The integration over positive values of x is restricted by eq. (2.31), and is non-zero only when $m_{c2(\text{high})}$ satisfies eqs. (2.30). If the lower bound on x is greater than zero, it will provide the lower limit of the integration. However, this is only the case when

$$m_{c2(\text{high})} > m_{c2(\text{eq})}^{\max} \quad (2.36)$$

which can never be true for Region 1 due to eq. (2.30), and there is only one permitted range:

$$0 < x < m_{c2(\text{high})}^2 \quad \text{for} \quad 0 < m_{c2(\text{high})} < m_{cb}^{\max}. \quad (2.37)$$

For the integral over negative values, x is restricted by eqs. (2.32) & (2.33). While the lower bound is unambiguous there are three possible upper bounds (including the original $x < 0$ from the integral) and we must divide the solution into three possible cases depending

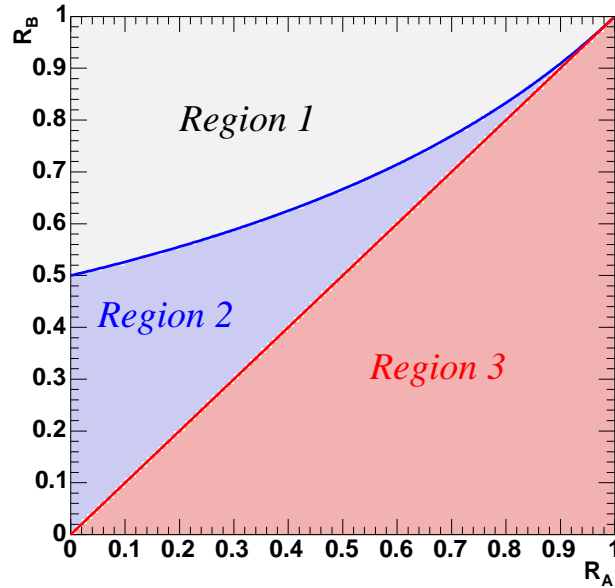


Figure 2: Regions 1, 2, and 3 vs. $R_A \equiv (m_A/m_B)^2$ and $R_B \equiv (m_B/m_C)^2$.

on which upper bound is dominant:

$$\begin{aligned}
-m_{c2(\text{high})}^2 < x < 0 & \quad \text{for } 0 < m_{c2(\text{high})} < m_{cb}^{\max}, \\
-m_{c2(\text{high})}^2 < x < (m_{cb}^{\max})^2 - m_{c2(\text{high})}^2 & \quad \text{for } m_{cb}^{\max} < m_{c2(\text{high})} < \frac{m_B}{m_C} m_{ca}^{\max}, \\
-m_{c2(\text{high})}^2 < x < \frac{(m_{cb}^{\max})^2}{a} - \left[\frac{(m_{cb}^{\max})^2}{a(m_{ca}^{\max})^2} + 1 \right] m_{c2(\text{high})}^2 & \quad \text{for } \frac{m_B}{m_C} m_{ca}^{\max} < m_{c2(\text{high})} < m_{ca}^{\max}.
\end{aligned} \tag{2.38}$$

Performing the two integrals in the appropriate cases and adding them together we find the full expression for the $m_{c2(\text{high})}^2$ distribution:

$$\frac{1}{\Gamma_0} \frac{\partial \Gamma_0}{\partial m_{c2(\text{high})}^2} = \begin{cases} \frac{1}{(m_{ca}^{\max})^2 a} \left[\ln \frac{(m_{cb}^{\max})^2}{(m_{cb}^{\max})^2 - a m_{c2(\text{high})}^2} + \frac{a m_{c2(\text{high})}^2}{(m_{cb}^{\max})^2 - a m_{c2(\text{high})}^2} \right] & \text{for } 0 < m_{c2(\text{high})} < m_{cb}^{\max}, \\ \frac{1}{(m_{ca}^{\max})^2 a} \ln \frac{m_C^2}{m_B^2} & \text{for } m_{cb}^{\max} < m_{c2(\text{high})} < \frac{m_B}{m_C} m_{ca}^{\max}, \\ \frac{1}{(m_{ca}^{\max})^2 a} \ln \frac{(m_{ca}^{\max})^2}{m_{c2(\text{high})}^2} & \text{for } \frac{m_B}{m_C} m_{ca}^{\max} < m_{c2(\text{high})} < m_{ca}^{\max}, \end{cases} \tag{2.39}$$

and zero otherwise.

2.2.2 Region 2: $R_A < R_B < \frac{1}{2-R_A}$

For Region 2 we have

$$\frac{m_B}{m_C} m_{ca}^{\max} < m_{c2(\text{eq})}^{\max} < m_{cb}^{\max} < m_{ca}^{\max}. \tag{2.40}$$

As for Region 1, the integration over positive x is restricted by eq. (2.31). However, *unlike* Region 1, the lower limit of eq. (2.31) can now be larger than zero, providing a new lower limit of integration. This happens when eq. (2.36) is satisfied, and provides different limits of integration for two distinct cases:

$$\begin{aligned}
0 < x < m_{c2(\text{high})}^2 & \quad \text{for } 0 < m_{c2(\text{high})} < m_{c2(\text{eq})}^{\max}, \\
\left[\frac{a(m_{ca}^{\max})^2}{(m_{cb}^{\max})^2} + 1 \right] m_{c2(\text{high})}^2 - (m_{ca}^{\max})^2 < x < m_{c2(\text{high})}^2 & \quad \text{for } m_{c2(\text{eq})}^{\max} < m_{c2(\text{high})} < m_{cb}^{\max}.
\end{aligned} \tag{2.41}$$

For the integration over negative x , the step-functions again require that eq. (2.32) and eq. (2.33) hold, if the integral is to be non-zero. However, since m_{cb}^{\max} is larger than $\frac{m_B}{m_C} m_{ca}^{\max}$ in Region 2, the upper bound from eq. (2.32) is never dominant. Therefore

Region 2 gives only two different sets of integration limits:

$$\begin{aligned}
& -m_{c2(\text{high})}^2 < x < 0 && \text{for } 0 < m_{c2(\text{high})} < m_{c2(\text{eq})}^{\max}, \\
& -m_{c2(\text{high})}^2 < x < \frac{(m_{cb}^{\max})^2}{a} - \left[\frac{(m_{cb}^{\max})^2}{a(m_{ca}^{\max})^2} + 1 \right] m_{c2(\text{high})}^2 && \text{for } m_{c2(\text{eq})}^{\max} < m_{c2(\text{high})} < m_{ca}^{\max}.
\end{aligned} \tag{2.42}$$

For Region 2 the full distribution is then given by

$$\frac{1}{\Gamma_0} \frac{\partial \Gamma_0}{\partial m_{c2(\text{high})}^2} = \begin{cases} \frac{1}{(m_{ca}^{\max})^2 a} \left[\ln \frac{(m_{cb}^{\max})^2}{(m_{cb}^{\max})^2 - am_{c2(\text{high})}^2} + \frac{am_{c2(\text{high})}^2}{(m_{cb}^{\max})^2 - am_{c2(\text{high})}^2} \right] & \text{for } 0 < m_{c2(\text{high})} < m_{c2(\text{eq})}^{\max}, \\ \frac{1}{(m_{ca}^{\max})^2 a} \left[\ln \frac{(m_{ca}^{\max})^2}{m_{c2(\text{high})}^2} + \frac{a(m_{ca}^{\max})^2}{(m_{cb}^{\max})^2} \right] & \text{for } m_{c2(\text{eq})}^{\max} < m_{c2(\text{high})} < m_{cb}^{\max}, \\ \frac{1}{(m_{ca}^{\max})^2 a} \ln \frac{(m_{ca}^{\max})^2}{m_{c2(\text{high})}^2} & \text{for } m_{cb}^{\max} < m_{c2(\text{high})} < m_{ca}^{\max}, \end{cases} \tag{2.43}$$

and zero otherwise.

2.2.3 Region 3: $0 < R_B < R_A$

In Region 3 we have

$$\frac{m_B}{m_C} m_{ca}^{\max} < m_{c2(\text{eq})}^{\max} < m_{ca}^{\max} < m_{cb}^{\max}. \tag{2.44}$$

For the individual integrations over positive and negative x , Region 3 is identical to Region 2, and we again obtain eqs. (2.41) & (2.42) for the positive and negative integration limits respectively. However, since m_{cb}^{\max} is now *larger* than m_{ca}^{\max} , contrary to Region 2, the sum of the two contributions will be different. We find:

$$\frac{1}{\Gamma_0} \frac{\partial \Gamma_0}{\partial m_{c2(\text{high})}^2} = \begin{cases} \frac{1}{(m_{ca}^{\max})^2 a} \left[\ln \frac{(m_{cb}^{\max})^2}{(m_{cb}^{\max})^2 - am_{c2(\text{high})}^2} + \frac{am_{c2(\text{high})}^2}{(m_{cb}^{\max})^2 - am_{c2(\text{high})}^2} \right] & \text{for } 0 < m_{c2(\text{high})} < m_{c2(\text{eq})}^{\max}, \\ \frac{1}{(m_{ca}^{\max})^2 a} \left[\ln \frac{(m_{ca}^{\max})^2}{m_{c2(\text{high})}^2} + \frac{a(m_{ca}^{\max})^2}{(m_{cb}^{\max})^2} \right] & \text{for } m_{c2(\text{eq})}^{\max} < m_{c2(\text{high})} < m_{ca}^{\max}, \\ \frac{1}{(m_{cb}^{\max})^2} & \text{for } m_{ca}^{\max} < m_{c2(\text{high})} < m_{cb}^{\max}, \end{cases} \tag{2.45}$$

and zero otherwise.

2.3 The two-particle invariant mass $m_{c2(\text{low})}$

The invariant mass $m_{c2(\text{low})}$ is given by

$$m_{c2(\text{low})} = \min(m_{cb}, m_{ca}). \quad (2.46)$$

For calculation of the differential decay rate we can adopt a method very similar to that of $m_{c2(\text{high})}$ above. Using u and v as defined in eq. (2.13) we can write $m_{c2(\text{low})}$ as

$$m_{c2(\text{low})}^2 = \min[(m_{cb}^{\text{max}})^2 u, (m_{ca}^{\text{max}})^2 (1 - au)v]. \quad (2.47)$$

Keeping x as defined in eq. (2.24), we write

$$m_{c2(\text{low})}^2 = \theta(-x)(m_{cb}^{\text{max}})^2 u + \theta(x)(m_{ca}^{\text{max}})^2 (1 - au)v. \quad (2.48)$$

These can be inverted to give

$$u = \frac{m_{c2(\text{low})}^2 + \theta(x)x}{(m_{cb}^{\text{max}})^2}, \quad v = \frac{m_{c2(\text{low})}^2 - \theta(-x)x}{(m_{ca}^{\text{max}})^2 \left(1 - a \frac{m_{c2(\text{low})}^2 + \theta(x)x}{(m_{cb}^{\text{max}})^2}\right)}, \quad (2.49)$$

and the differential distribution again has the form (2.27), but now with

$$u_- = \frac{m_{c2(\text{low})}^2}{(m_{cb}^{\text{max}})^2}, \quad u_+ = \frac{m_{c2(\text{low})}^2 + x}{(m_{cb}^{\text{max}})^2}, \quad (2.50)$$

$$v_- = \frac{m_{c2(\text{low})}^2 - x}{(m_{ca}^{\text{max}})^2 \left(1 - a \frac{m_{c2(\text{low})}^2}{(m_{cb}^{\text{max}})^2}\right)}, \quad v_+ = \frac{m_{c2(\text{low})}^2}{(m_{ca}^{\text{max}})^2 \left(1 - a \frac{m_{c2(\text{low})}^2 + x}{(m_{cb}^{\text{max}})^2}\right)}. \quad (2.51)$$

These are actually the same definitions as eqs. (2.28) and (2.29) only now written in terms of $m_{c2(\text{low})}$ rather than $m_{c2(\text{high})}$, using

$$|x| = m_{c2(\text{high})}^2 - m_{c2(\text{low})}^2, \quad (2.52)$$

as follows from (2.23), (2.24) and (2.47). The step-functions of the integrand then give the following restrictions on x and/or $m_{c2(\text{low})}$:

$$\hat{\theta}(u_+) \neq 0 \Rightarrow -m_{c2(\text{low})}^2 < x < (m_{cb}^{\text{max}})^2 - m_{c2(\text{low})}^2, \quad (2.53)$$

$$\hat{\theta}(v_+) \neq 0 \Rightarrow x < \frac{(m_{cb}^{\text{max}})^2}{a} - \left[\frac{(m_{cb}^{\text{max}})^2}{a(m_{ca}^{\text{max}})^2} + 1\right] m_{c2(\text{low})}^2, \quad (2.54)$$

$$\hat{\theta}(u_-) \neq 0 \Rightarrow 0 < m_{c2(\text{low})} < m_{cb}^{\text{max}}, \quad (2.55)$$

$$\hat{\theta}(v_-) \neq 0 \Rightarrow \left[\frac{a(m_{ca}^{\text{max}})^2}{(m_{cb}^{\text{max}})^2} + 1\right] m_{c2(\text{low})}^2 - (m_{ca}^{\text{max}})^2 < x < m_{c2(\text{low})}^2. \quad (2.56)$$

The parallels with the $m_{c2(\text{high})}$ case are obvious. The step-functions provide the same constraints for $m_{c2(\text{low})}$ as they did for $m_{c2(\text{high})}$, but constraints which were previously for negative x are now for positive x and vice versa. Therefore we must be careful with the $x = 0$ boundary: we will have the same regions of applicability as shown in figure 2 but the inequalities giving the integration limits for each region will be different from the $m_{c2(\text{high})}$ case.

2.3.1 Region 1: $\frac{1}{2-R_A} < R_B < 1$

In Region 1, eq. (2.35) holds as before.

For positive x , we have constraints given by eqs. (2.53) & (2.54). However, in Region 1 the upper bound on x provided by eq. (2.53) is always more restrictive, and insists that $m_{c2(\text{low})}$ be smaller than m_{cb}^{max} for a nonzero result. Finally, since $m_{c2(\text{low})}^2$ is necessarily positive, the lower bound on x is trivially zero. Therefore, the integration limits for Region 1 with positive x only has one case:

$$0 < x < (m_{cb}^{\text{max}})^2 - m_{c2(\text{low})}^2 \quad \text{for } 0 < m_{c2(\text{low})} < m_{cb}^{\text{max}}. \quad (2.57)$$

For negative x , the integration limits also only have one case since eq. (2.55) restricts $m_{c2(\text{low})}$ to be below all the characteristic masses in eq. (2.35). This gives

$$-(m_{ca}^{\text{max}})^2 + \left[\frac{a(m_{ca}^{\text{max}})^2}{(m_{cb}^{\text{max}})^2} + 1 \right] m_{c2(\text{low})}^2 < x < 0 \quad \text{for } 0 < m_{c2(\text{low})} < m_{cb}^{\text{max}}. \quad (2.58)$$

It is then rather trivial to calculate the full integral for Region 1:

$$\frac{1}{\Gamma_0} \frac{\partial \Gamma_0}{\partial m_{c2(\text{low})}^2} = \frac{1}{(m_{ca}^{\text{max}})^2 a} \left[\ln \frac{(m_{cb}^{\text{max}})^2 - a m_{c2(\text{low})}^2}{\frac{m_B^2}{m_C} (m_{cb}^{\text{max}})^2} + \frac{a(m_{ca}^{\text{max}})^2}{(m_{cb}^{\text{max}})^2} - \frac{a m_{c2(\text{low})}^2}{(m_{cb}^{\text{max}})^2 - a m_{c2(\text{low})}^2} \right], \quad (2.59)$$

for $0 < m_{c2(\text{low})} < m_{cb}^{\text{max}}$, and zero otherwise.

2.3.2 Regions 2 and 3: $0 < R_B < \frac{1}{2-R_A}$

The inequalities given by the step-functions together with the positivity or negativity constraints on x , are independent of the boundary between Regions 2 and 3. In other words, which of m_{ca}^{max} and m_{cb}^{max} is larger is irrelevant when both are larger than $m_{c2(\text{eq})}^{\text{max}}$. Therefore the analytic form of the distribution will be the same in Region 2 as it is in Region 3 and we do not need to treat them separately. The hierarchy of characteristic masses is then:

$$\frac{m_B}{m_C} m_{ca}^{\text{max}} < m_{c2(\text{eq})}^{\text{max}} < \min(m_{ca}^{\text{max}}, m_{cb}^{\text{max}}) \quad (2.60)$$

For positive x , the issue is which of the upper bounds of eqs. (2.53) & (2.54) is more restrictive. For higher values of $m_{c2(\text{low})}$ it is eq. (2.54) which is more restrictive, with the transition being at $\frac{m_B}{m_C} m_{ca}^{\text{max}}$ as already intimated by eq. (2.38), and we must also ensure that this upper bound on x is positive. Together, these considerations give the integration limits:

$$\begin{aligned} 0 < x < (m_{cb}^{\text{max}})^2 - m_{c2(\text{low})}^2 & \quad \text{for } 0 < m_{c2(\text{low})} < \frac{m_B}{m_C} m_{ca}^{\text{max}}, \\ 0 < x < \frac{(m_{cb}^{\text{max}})^2}{a} - \left[\frac{(m_{cb}^{\text{max}})^2}{a(m_{ca}^{\text{max}})^2} + 1 \right] m_{c2(\text{low})}^2 & \quad \text{for } \frac{m_B}{m_C} m_{ca}^{\text{max}} < m_{c2(\text{low})} < m_{c2(\text{eq})}^{\text{max}}. \end{aligned} \quad (2.61)$$

For negative x , only the (lower) constraint of eq. (2.56) is interesting. The insistence that this lower bound is negative requires that $m_{c2(\text{low})}$ is smaller than $m_{c2(\text{eq})}^{\text{max}}$, which is more restrictive than eq. (2.55) for these regions. The integration limits for negative x are therefore again rather simple:

$$-(m_{ca}^{\text{max}})^2 + \left[\frac{a(m_{ca}^{\text{max}})^2}{(m_{cb}^{\text{max}})^2} + 1 \right] m_{c2(\text{low})}^2 < x < 0 \quad \text{for } 0 < m_{c2(\text{low})} < m_{c2(\text{eq})}^{\text{max}}. \quad (2.62)$$

The full result for Regions 2 and 3 is:

$$\frac{1}{\Gamma_0} \frac{\partial \Gamma_0}{\partial m_{c2(\text{low})}^2} = \left\{ \begin{array}{l} \frac{1}{(m_{ca}^{\text{max}})^2 a} \left[\ln \frac{(m_{cb}^{\text{max}})^2 - am_{c2(\text{low})}^2}{\frac{m_B^2}{m_C^2} (m_{cb}^{\text{max}})^2} + \frac{a(m_{ca}^{\text{max}})^2}{(m_{cb}^{\text{max}})^2} - \frac{am_{c2(\text{low})}^2}{(m_{cb}^{\text{max}})^2 - am_{c2(\text{low})}^2} \right] \\ \quad \text{for } 0 < m_{c2(\text{low})} < \frac{m_B}{m_C} m_{ca}^{\text{max}}, \\ \\ \frac{1}{(m_{ca}^{\text{max}})^2 a} \left[\ln \frac{(m_{ca}^{\text{max}})^2 [(m_{cb}^{\text{max}})^2 - am_{c2(\text{low})}^2]}{(m_{cb}^{\text{max}})^2 m_{c2(\text{low})}^2} + \frac{a(m_{ca}^{\text{max}})^2}{(m_{cb}^{\text{max}})^2} - \frac{am_{c2(\text{low})}^2}{(m_{cb}^{\text{max}})^2 - am_{c2(\text{low})}^2} \right] \\ \quad \text{for } \frac{m_B}{m_C} m_{ca}^{\text{max}} < m_{c2(\text{low})} < m_{c2(\text{eq})}^{\text{max}}, \end{array} \right. \quad (2.63)$$

and zero otherwise.

2.4 The three-particle invariant mass m_{cba}

The quantity m_{cba} is defined by

$$m_{cba}^2 \equiv (p_c + p_b + p_a)^2. \quad (2.64)$$

Making use of energy and momentum conservation, we can write this in terms of particle masses and two angles:

$$m_{cba}^2 = m_D^2 - m_B^2 - y \left(\frac{m_B^2 + m_A^2}{m_B} \right) + \sqrt{y^2 + 2ym_B + m_B^2 - m_D^2} \left(\frac{m_B^2 - m_A^2}{m_B} \right) (1 - 2w), \quad (2.65)$$

where u is given by eq. (2.13), w is similarly defined in terms of the angle between A and D in the rest frame of B ,

$$w \equiv \frac{1 - \cos \theta_{AD}^{(B)}}{2}, \quad (2.66)$$

and the quantity y is defined by

$$y \equiv \frac{(m_D^2 - m_B^2) m_B}{2m_C^2} u + \frac{(m_C^2 - m_B^2)^2}{2m_B m_C^2} u + \left(\frac{m_D^2 - m_B^2}{2m_B} \right) (1 - u). \quad (2.67)$$

It is straightforward to solve for u and w ,

$$u = \frac{(m_D^2 - m_B^2) m_C^2 - 2m_C^2 m_B y}{(m_D^2 - m_C^2) (m_C^2 - m_B^2)},$$

$$w = \frac{m_D^2 - m_B^2 - y \left(\frac{m_B^2 + m_A^2}{m_B} \right) + \sqrt{y^2 + 2ym_B + m_B^2 - m_D^2} \left(\frac{m_B^2 - m_A^2}{m_B} \right) - m_{cba}^2}{2\sqrt{y^2 + 2ym_B + m_B^2 - m_D^2} \left(\frac{m_B^2 - m_A^2}{m_B} \right)}. \quad (2.68)$$

Under the assumption that B is a scalar particle, its decay is isotropic and the doubly-differential width in terms of these two variables u and w must be flat. Therefore we can write

$$\begin{aligned} \frac{1}{\Gamma_0} \frac{\partial^2 \Gamma_0}{\partial y \partial m_{cba}^2} &= \left| \frac{\partial(u, w)}{\partial(y, m_{cba}^2)} \right| \frac{1}{\Gamma_0} \frac{\partial^2 \Gamma_0}{\partial u \partial w} \\ &= \frac{m_C^2 m_B^2}{(m_D^2 - m_C^2) (m_C^2 - m_B^2) (m_B^2 - m_A^2)} \frac{\hat{\theta}(u) \hat{\theta}(w)}{\sqrt{y^2 + 2ym_B + m_B^2 - m_D^2}} \end{aligned} \quad (2.69)$$

and integrate over y to acquire the desired distribution,

$$\frac{1}{\Gamma_0} \frac{\partial \Gamma_0}{\partial m_{cba}^2} = \frac{1}{(m_{ca}^{\max})^2 a} \int_{-\infty}^{\infty} \frac{\hat{\theta}(u) \hat{\theta}(w)}{\sqrt{y^2 + 2ym_B + m_B^2 - m_D^2}} dy. \quad (2.70)$$

At this point it is useful to make some definitions, in order to help keep expressions compact. Let us first define the integral:

$$\begin{aligned} L(a_1, a_2) &\equiv \int_{a_1}^{a_2} \frac{1}{\sqrt{y^2 + 2ym_B + m_B^2 - m_D^2}} dy \\ &= \ln \frac{a_2 + m_B + \sqrt{a_2^2 + 2a_2 m_B + m_B^2 - m_D^2}}{a_1 + m_B + \sqrt{a_1^2 + 2a_1 m_B + m_B^2 - m_D^2}}, \end{aligned} \quad (2.71)$$

which is the only integral that we will need. The mass values which appear as kinematical endpoints of m_{cba} are [10, 12]:

$$m_1^2 = \frac{(m_D^2 - m_C^2) (m_C^2 - m_A^2)}{m_C^2}, \quad (2.72)$$

$$m_2^2 = \frac{(m_C^2 - m_B^2)(m_D^2 m_B^2 - m_C^2 m_A^2)}{m_B^2 m_C^2}, \quad (2.73)$$

$$m_3^2 = \frac{(m_D^2 - m_B^2)(m_B^2 - m_A^2)}{m_B^2}, \quad (2.74)$$

$$m_4^2 = (m_D - m_A)^2. \quad (2.75)$$

The mass m_4 is always the largest, as is seen by

$$\begin{aligned} m_4^2 - m_1^2 &= (m_C^2 - m_A m_D)^2 / m_C^2, \\ m_4^2 - m_2^2 &= (m_B^2 m_D - m_A m_C^2)^2 / (m_B^2 m_C^2), \\ m_4^2 - m_3^2 &= (m_B^2 - m_A m_D)^2 / m_B^2. \end{aligned} \quad (2.76)$$

For the others, the relative order will depend on the values of m_A , m_B , m_C , and m_D :

$$\begin{aligned} m_1^2 - m_2^2 &= (m_B^2 - m_A^2)(m_B^2 m_D^2 - m_C^2 m_C^2) / (m_B^2 m_C^2), \\ m_1^2 - m_3^2 &= (m_C^2 - m_B^2)(m_A^2 m_D^2 - m_B^2 m_C^2) / (m_B^2 m_C^2), \\ m_2^2 - m_3^2 &= (m_D^2 - m_C^2)(m_A^2 m_C^2 - m_B^2 m_B^2) / (m_B^2 m_C^2). \end{aligned} \quad (2.77)$$

As for the previous distributions, it is important to determine the upper and lower integration bounds. The step-functions for u provide rather simple constraints,

$$y_1 \equiv \frac{m_D^2 - m_B^2 - (m_{cb}^{\max})^2}{2m_B} < y < \frac{m_D^2 - m_B^2}{2m_B} \equiv y_2, \quad (2.78)$$

where we have defined the quantities $y_{1,2}$ for later convenience. The constraints from the step-functions for w are somewhat more complicated,

$$y_3 < y < y_4, \quad (2.79)$$

where

$$\begin{aligned} y_{4,3} \equiv \frac{1}{4m_B m_A^2} \left\{ (m_B^2 - m_A^2)^2 - [m_{cba}^2 - (m_D^2 - m_B^2)](m_B^2 + m_A^2) \right. \\ \left. \pm (m_B^2 - m_A^2) \sqrt{(m_D^2 - m_A^2 - m_{cba}^2)^2 - 4m_A^2 m_{cba}^2} \right\}. \end{aligned} \quad (2.80)$$

In order that $y_{4,3}$ be real, we must insist that $m_{cba} < m_4$, with m_4 defined by eq. (2.75).

We now need to compare these constraints and determine the relative ordering of y_1 , y_2 , y_3 and y_4 , to see which will form the endpoints of the y integration. There are four possible cases where the constraints overlap, as illustrated in figure 3.

y_1 vs. y_4 : In order to have a physical solution, we require that $y_1 < y_4$. This constraint is manifest differently for different mass hierarchies. Comparing the expressions from eqs. (2.78) & (2.80) we find the requirements,

$$\begin{aligned} \text{for } m_C^2 < m_A m_D \ (\Rightarrow m_A m_C^2 < m_B^2 m_D), \quad y_1 < y_4 \text{ if } m_{cba} < m_1, \\ \text{for } m_C^2 > m_A m_D \ \& \ m_A m_C^2 > m_B^2 m_D, \quad y_1 < y_4 \text{ if } m_{cba} < m_2, \\ \text{for } m_C^2 > m_A m_D \ \& \ m_A m_C^2 < m_B^2 m_D, \quad y_1 < y_4 \text{ if } m_{cba} < m_4, \end{aligned} \quad (2.81)$$

where m_1 , m_2 and m_4 are given by eqs. (2.72), (2.73) & (2.75) respectively.

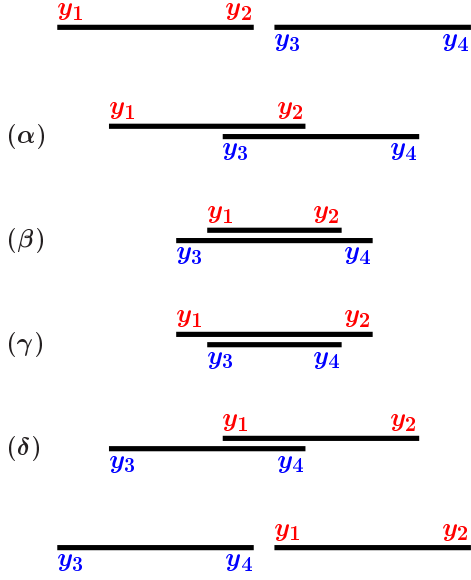


Figure 3: Schematic representation of integration ranges. The cases (α)–(δ) give non-zero contributions.

y_2 vs. y_3 : Similarly, to provide an overlap of the integration regions we must insist that $y_2 > y_3$. Once again, which values of m_{cba} are required is dependent on the mass hierarchy:

$$\begin{aligned} \text{for } m_B^2 < m_A m_D, \quad y_3 < y_2 \text{ if } m_{cba} < m_4, \\ \text{for } m_B^2 > m_A m_D, \quad y_3 < y_2 \text{ if } m_{cba} < m_3, \end{aligned} \quad (2.82)$$

where m_3 is given by eq. (2.74).

y_2 vs. y_4 : Although one does not require any particular relation between y_2 and y_4 in order to have a non-zero result, only the smallest of y_2 and y_4 will provide the upper bound on the integration, so it is important to verify which mass regimes lead to which dominant upper bound. We find:

$$\begin{aligned} \text{for } m_B^2 < m_A m_D, \quad y_2 < y_4 \text{ if } m_{cba} < m_3, \\ \text{for } m_B^2 > m_A m_D, \quad y_2 < y_4 \text{ if } m_{cba} < m_4. \end{aligned} \quad (2.83)$$

y_1 vs. y_3 : Finally, the lower bound of the integration is governed by whichever of y_1 and y_3 is larger. We find:

$$\begin{aligned} \text{for } m_C^2 < m_A m_D \quad (\Rightarrow m_A m_C^2 < m_B^2 m_D), \quad y_1 > y_3 \text{ if } m_2 < m_{cba} < m_4, \\ \text{for } m_C^2 > m_A m_D \quad \& \quad m_A m_C^2 > m_B^2 m_D, \quad y_1 > y_3 \text{ if } m_1 < m_{cba} < m_4, \\ \text{for } m_C^2 > m_A m_D \quad \& \quad m_A m_C^2 < m_B^2 m_D, \\ y_1 > y_3 \text{ if } \min(m_1, m_2) < m_{cba} < \max(m_1, m_2). \end{aligned} \quad (2.84)$$

As for the simpler two-particle invariant masses, the mass-dependent relations obtained above result in different distributions in different regions of mass-space. We must therefore specify the mass hierarchy of these regions before continuing. Given the ordering of eq. (1.4), an unambiguous division² is:

$$\text{Region 1: } \underline{m_C^2 < m_A m_D}, \quad m_A m_C^2 < m_B^2 m_D, \quad m_B^2 < m_A m_D \quad (2.85)$$

$$\text{Region 2: } m_C^2 > m_A m_D, \quad \underline{m_A m_C^2 > m_B^2 m_D}, \quad m_B^2 < m_A m_D \quad (2.86)$$

$$\text{Region 3: } m_C^2 > m_A m_D, \quad m_A m_C^2 < m_B^2 m_D, \quad \underline{m_B^2 > m_A m_D} \quad (2.87)$$

$$\text{Region 4: } m_C^2 > m_A m_D, \quad m_A m_C^2 < m_B^2 m_D, \quad m_B^2 < m_A m_D \quad (2.88)$$

²Note that the ‘regions’ defined here are different from those of sects. 2.2 and 2.3. The present ones are three-dimensional volumes, whereas those of sects. 2.2 and 2.3 are two-dimensional areas.

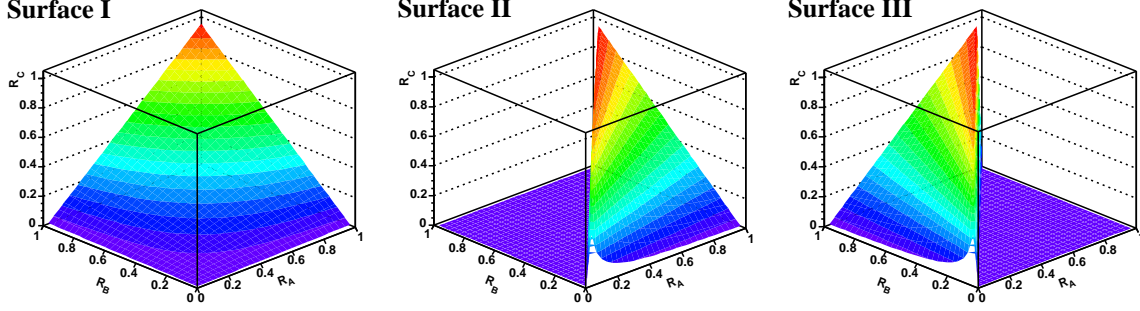


Figure 4: Allowed values of R_A , R_B and R_C for the four main regions of m_{cba} in terms of volumes inside the unit cube. The allowed values for Region 1 lie in the volume below Surface I: $0 < R_C < R_A R_B < 1$. For Region 2 the allowed volume is that above Surface II: $0 < \frac{R_B}{R_A} < R_C < 1$ (not including the flat region where $R_B > R_A$). Likewise the allowed volume for Region 3 is that above Surface III: $0 < \frac{R_A}{R_B} < R_C < 1$. Region 4 lies in the volume above Surface I and below Surfaces II and III. (See figure 12 for projections onto the R_A - R_B -plane).

This division, in terms of the mass ratios of eq. (2.34), is illustrated in figure 4, and has the property that each region has a different endpoint for the invariant mass distribution. The different orderings of m_1 , m_2 and m_3 , as given by eq. (2.77), will lead to further subdivisions of the above regions.

2.4.1 Region 1: $0 < R_C < R_A R_B < 1$

The first inequality (underlined) of eq. (2.85) implies the other two hold for our mass hierarchy. Also, as seen from (2.76) and (2.77), since $m_C^2 < m_A m_D < m_B m_D$ and $m_B^2 m_C^2 < m_C^4 < m_A^2 m_D^2$, we have $m_2 < m_1 < m_4$ and $m_3 < m_1 < m_4$ respectively, but the relative size of m_2 and m_3 is undetermined. Thus, we must divide the region into subregions.

Region (1,1): If $m_B^2 > m_A m_C$ then $m_2 < m_3 < m_1$ (see eq. (2.77)), and we find the invariant mass distribution is, in terms of the function L defined in eq. (2.71),

$$\frac{1}{\Gamma_0} \frac{\partial \Gamma_0}{\partial m_{cba}^2} = \frac{1}{(m_{ca}^{\max})^2 a} \begin{cases} L(y_3, y_2) & \text{for } 0 < m_{cba} < m_2, \\ L(y_1, y_2) & \text{for } m_2 < m_{cba} < m_3, \\ L(y_1, y_4) & \text{for } m_3 < m_{cba} < m_1, \end{cases} \quad (2.89)$$

and zero otherwise.

Region (1,2): Alternatively, if $m_B^2 < m_A m_C$ then $m_3 < m_2 < m_1$ and the invariant mass distribution is:

$$\frac{1}{\Gamma_0} \frac{\partial \Gamma_0}{\partial m_{cba}^2} = \frac{1}{(m_{ca}^{\max})^2 a} \begin{cases} L(y_3, y_2) & \text{for } 0 < m_{cba} < m_3, \\ L(y_3, y_4) & \text{for } m_3 < m_{cba} < m_2, \\ L(y_1, y_4) & \text{for } m_2 < m_{cba} < m_1, \end{cases} \quad (2.90)$$

and zero otherwise.

2.4.2 Region 2: $0 < \frac{R_B}{R_A} < R_C < 1$

In this region, the second inequality (underlined) of eq. (2.86) implies the other two. Also, since $m_B m_D < m_C^2$ and $m_B^2 < \frac{m_D}{m_C} m_B^2 < m_A m_C$ we have $m_1 < m_2$ and $m_3 < m_2$, but the relative magnitude of m_1 and m_3 is undetermined and we must divide our region in two.

Region (2,1): If $m_A m_D < m_B m_C$ then $m_1 < m_3 < m_2$ (see eq. (2.77)), and we find the invariant mass distribution is:

$$\frac{1}{\Gamma_0} \frac{\partial \Gamma_0}{\partial m_{cba}^2} = \frac{1}{(m_{ca}^{\max})^2 a} \begin{cases} L(y_3, y_2) & \text{for } 0 < m_{cba} < m_1, \\ L(y_1, y_2) & \text{for } m_1 < m_{cba} < m_3, \\ L(y_1, y_4) & \text{for } m_3 < m_{cba} < m_2, \end{cases} \quad (2.91)$$

and zero otherwise.

Region (2,2): If $m_A m_D > m_B m_C$ then $m_3 < m_1 < m_2$, and the distribution is:

$$\frac{1}{\Gamma_0} \frac{\partial \Gamma_0}{\partial m_{cba}^2} = \frac{1}{(m_{ca}^{\max})^2 a} \begin{cases} L(y_3, y_2) & \text{for } 0 < m_{cba} < m_3, \\ L(y_3, y_4) & \text{for } m_3 < m_{cba} < m_1, \\ L(y_1, y_4) & \text{for } m_1 < m_{cba} < m_2, \end{cases} \quad (2.92)$$

and zero otherwise.

2.4.3 Region 3: $0 < \frac{R_A}{R_B} < R_C < 1$

In this region, it is the third inequality (underlined) which leads to the other two. The inequalities $m_A m_C < m_A m_D < m_B^2$ and $m_A m_D < m_B m_C$ tell us that $m_2 < m_3$ and $m_1 < m_3$. Although we do not know the order of m_1 and m_2 , the endpoints of the integration are independent of which one is larger and their relative magnitude only affects the region of applicability of the different functions (unlike in Regions 1 and 2 where the integration endpoints also changed). For the entirety of Region 3 we find:

$$\frac{1}{\Gamma_0} \frac{\partial \Gamma_0}{\partial m_{cba}^2} = \frac{1}{(m_{ca}^{\max})^2 a} \begin{cases} L(y_3, y_2) & \text{for } 0 < m_{cba} < \min(m_1, m_2), \\ L(y_1, y_2) & \text{for } \min(m_1, m_2) < m_{cba} < \max(m_1, m_2), \\ L(y_3, y_2) & \text{for } \max(m_1, m_2) < m_{cba} < m_3, \end{cases} \quad (2.93)$$

and zero otherwise. Note that $m_1 < m_2$ when $m_B m_D < m_C^2$, from eq. (2.77).

2.4.4 Region 4: $0 < R_A R_B < R_C$ and $R_C < \frac{R_B}{R_A} < 1$ and $R_C < \frac{R_A}{R_B} < 1$

Region 4 encompasses all the other allowed areas of mass-space. In this region we only know, *a priori*, that m_1, m_2 and m_3 are smaller than m_4 (as for all regions) but not their

relative sizes. However, as for Region 3, the ordering of m_1 and m_2 does not change the endpoints of the integration, but only changes the region of applicability. Therefore, we have three possible subregions, corresponding to the relative sizes of m_3 and the maximum and minimum of m_1 and m_2 .

Region (4,1): If $m_A m_D > m_B m_C$ and $m_B^2 < m_A m_C$ then $m_3 < \min(m_1, m_2)$, and the invariant mass distribution is:

$$\frac{1}{\Gamma_0} \frac{\partial \Gamma_0}{\partial m_{cba}^2} = \frac{1}{(m_{ca}^{\max})^2 a} \begin{cases} L(y_3, y_2) & \text{for } 0 < m_{cba} < m_3, \\ L(y_3, y_4) & \text{for } m_3 < m_{cba} < \min(m_1, m_2), \\ L(y_1, y_4) & \text{for } \min(m_1, m_2) < m_{cba} < \max(m_1, m_2), \\ L(y_3, y_4) & \text{for } \max(m_1, m_2) < m_{cba} < m_4, \end{cases} \quad (2.94)$$

and zero otherwise.

Region (4,2): If $\{m_B m_D > m_C^2, m_A m_D > m_B m_C \text{ and } m_B^2 > m_A m_C\}$ **or** $\{m_B m_D < m_C^2, m_A m_D < m_B m_C \text{ and } m_B^2 < m_A m_C\}$ then $\min(m_1, m_2) < m_3 < \max(m_1, m_2)$, and the invariant mass distribution is:

$$\frac{1}{\Gamma_0} \frac{\partial \Gamma_0}{\partial m_{cba}^2} = \frac{1}{(m_{ca}^{\max})^2 a} \begin{cases} L(y_3, y_2) & \text{for } 0 < m_{cba} < \min(m_1, m_2), \\ L(y_1, y_2) & \text{for } \min(m_1, m_2) < m_{cba} < m_3, \\ L(y_1, y_4) & \text{for } m_3 < m_{cba} < \max(m_1, m_2), \\ L(y_3, y_4) & \text{for } \max(m_1, m_2) < m_{cba} < m_4, \end{cases} \quad (2.95)$$

and zero otherwise.

Region (4,3): Finally, if $m_A m_D < m_B m_C$ and $m_B^2 > m_A m_C$ then $\max(m_1, m_2) < m_3$, and the invariant mass distribution is:

$$\frac{1}{\Gamma_0} \frac{\partial \Gamma_0}{\partial m_{cba}^2} = \frac{1}{(m_{ca}^{\max})^2 a} \begin{cases} L(y_3, y_2) & \text{for } 0 < m_{cba} < \min(m_1, m_2), \\ L(y_1, y_2) & \text{for } \min(m_1, m_2) < m_{cba} < \max(m_1, m_2), \\ L(y_3, y_2) & \text{for } \max(m_1, m_2) < m_{cba} < m_3, \\ L(y_3, y_4) & \text{for } m_3 < m_{cba} < m_4, \end{cases} \quad (2.96)$$

and zero otherwise.

3. Parton level

In order to explore how the derived expressions can be applied to real data, we will compare with SUSY cascade decays in Monte Carlo (MC) events generated for the mSUGRA Snowmass benchmark point SPS 1a [14]. SPS 1a has the GUT scale parameters $m_0 = 100$ GeV,

$m_{1/2} = 250$ GeV, $A_0 = -100$ GeV, $\tan\beta = 10$ and $\mu > 0$. The TeV-scale SUSY mass spectrum is calculated from these parameters, together with a top mass of $m_t = 175$ GeV, by ISAJET 7.58 [22] (for numerical values, see, e.g. [12]). We have generated a number of events equivalent to 50 fb^{-1} at the LHC, by running PYTHIA 6.208 [17] with CTEQ 5L parton distribution functions [23].

In particular, we focus on the decay chain (1.1), which was previously investigated in some detail in [12]. The comparison is done for the invariant masses $m_{ql(\text{low})}$, $m_{ql(\text{high})}$, m_{ql_f} and m_{qll} .³ For the quark q we consider only the up quark and the corresponding squark. The complications introduced with more than one flavour, and thus multiple, overlaying distributions, will be faced in the next section.

We find the analytic expressions for the distributions by going from the distribution of the square of the invariant mass to the distribution of the invariant mass by eq. (2.21) and substituting $A = \tilde{\chi}_1^0$, $B = \tilde{l}_R$, $C = \tilde{\chi}_2^0$ and $D = \tilde{u}_L$ in our expressions.

However, this simple picture is not what will be seen in an actual experiment. The shapes will be distorted by the width of the SUSY particles, cuts applied to remove backgrounds, by Final State Radiation (FSR), and by detector effects. In order to use the shapes for extracting NP particle masses from real data it is important to understand these effects, and the limits they place on the use of the shapes. Here we consider the three main effects apparent at parton level, width effects, the bias introduced by cuts and a shift in invariant mass from FSR.

3.1 Width

Since we have not taken into account the width of the decaying particles we additionally smear the analytic expression with a (truncated) Breit-Wigner function. If $g(m)$ is the original distribution we plot in the following figures the function $f(m)$ given by the convolution

$$f(m) = \frac{\Gamma_s}{4 \arctan 20} \int_{m-10\Gamma_s}^{m+10\Gamma_s} \frac{g(m')}{(m' - m)^2 + (\Gamma_s/2)^2} dm', \quad (3.1)$$

where Γ_s is a parameter of the smearing, determined by a fit to the MC data. We normalize the analytic expression to the number of MC events.

The smeared analytic curves (for the SPS 1a parameters) are compared with the parton level MC distributions, with no cuts or Final State Radiation, in figure 5. The agreement is very good, being at the level expected from statistical fluctuations in the MC, and provides a verification of our analytic expressions. The smearing is responsible for a rounding of the sharp peaks in the $m_{ql(\text{low})}$ and m_{cba} distributions, and greatly improves agreement near the upper end of the distributions.

3.2 Cuts

We apply the cuts used in [12] to isolate the decay chain from Standard Model background,

- the three hardest jets have $p_T^{\text{jet}} > 150, 100, 50$ GeV,

³We include the distribution of m_{ql_f} for comparison with our analytical expression, even though it will be difficult to separate the near and far leptons experimentally.

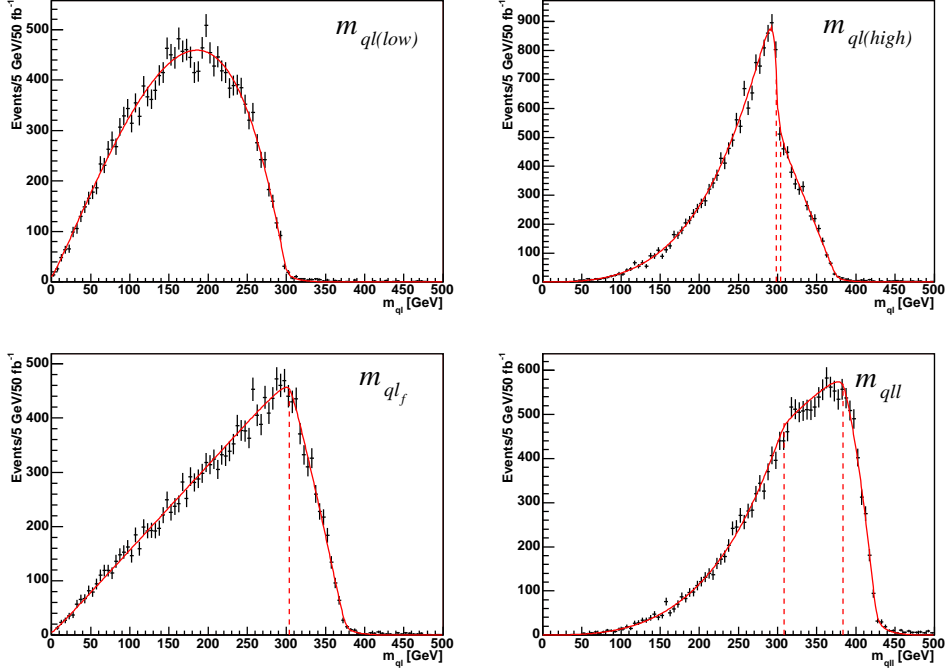


Figure 5: Invariant mass distributions at parton level with no cuts and no FSR. MC events (black) are shown with errors. The lines (red) are the analytic expressions with nominal masses. The dashed lines show the ranges of validity of the different function pieces.

- $E_{T,\text{miss}} > \max(100 \text{ GeV}, 0.2 M_{\text{eff}})$, where $M_{\text{eff}} \equiv E_{T,\text{miss}} + \sum_{i=1}^3 p_{T,i}^{\text{jet}}$,
- the two hardest leptons have $p_T^{\text{lep}} > 20, 10 \text{ GeV}$.

Figure 6 compares the analytic curves with the parton level MC events after the application of these cuts. From a visual inspection we see a fairly good agreement between the MC events and the analytic functions, except that the number of events at low invariant mass is reduced in the MC distribution compared to the analytic curve. This is most pronounced for $m_{ql(\text{low})}$.

In order to determine which of the cuts is introducing this discrepancy, we show in figure 7 the average value of the cut variables $E_{T,\text{miss}} - \max(100, 0.2M_{\text{eff}})$, $p_{T,1}^{\text{lep}}$, $p_{T,2}^{\text{lep}}$ and $p_{T,1}^{\text{jet}}$, in each bin of the $m_{ql(\text{low})}$ invariant mass distribution versus the invariant mass in that bin. The two jet cuts omitted have a very similar behaviour to that on the hardest jet.

For the cut on missing energy there is a large gap between the signals's missing energy and the cut value (except for the two end bins, where low statistics lead to large errors) and therefore the effects on the shape of the invariant mass distribution will be small. On the other hand, because of the small difference between the cut value and the average value at low invariant masses, the cut on the transverse momentum of the second hardest lepton, $p_{T,2}^{\text{lep}}$, will clearly introduce a bias by removing more events at low invariant masses. From figure 7 we see that we should be safe in trusting the analytic shape of the distribution

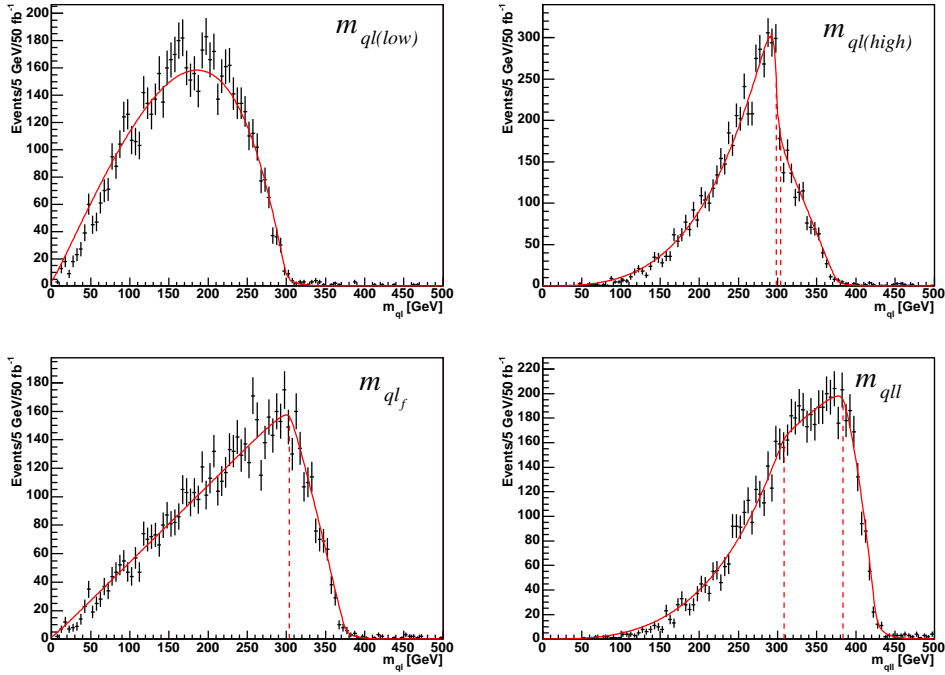


Figure 6: Invariant mass distributions at parton level with cuts as described in the text, but no FSR. MC events (black) are shown with errors. The lines (red) are the analytic expressions with nominal masses. The dashed lines show the ranges of validity of the different function pieces.

after the cut on $p_{T,2}^{\text{lep}}$, down to around $m_{ql(\text{low})} = 100 - 150$ GeV where the $p_{T,2}^{\text{lep}}$ distribution flattens out due to the cut imposed. The cut on the transverse momentum of the hardest lepton, $p_{T,1}^{\text{lep}}$, will likewise have some effect on the distribution, but only at very low invariant masses. For the cut on transverse momentum of the hardest jet, and similarly for the other two jet cuts, we again find that the average values do not lie close enough to the cut value, for most of the invariant mass bins, to cause a problem. However, even if this had not been the case, since the average value of $p_{T,1}^{\text{jet}}$ as a function of $m_{ql(\text{low})}$ is to a good approximation flat, it would have cut equally at all invariant mass values, and so introduced no bias.

Studying the average of a cut variable over the range of possible invariant mass values enables us to give an estimate of where it is safe to fit the distributions given some cut value, and could also be used to optimize the cuts so that they introduce less or no bias for certain ranges of invariant mass.

3.3 Final state radiation

In figure 8 we include FSR in the MC data and we observe a slight shift towards lower invariant masses for all four distributions as compared to the analytic shape. This can be compared with figure 6 which included no FSR.

Ignoring statistical fluctuations between the two different event samples this shows that FSR conserves the shape of the distributions, but lowers the invariant masses slightly, indicating that it should be possible to use the shape of the distributions in determining

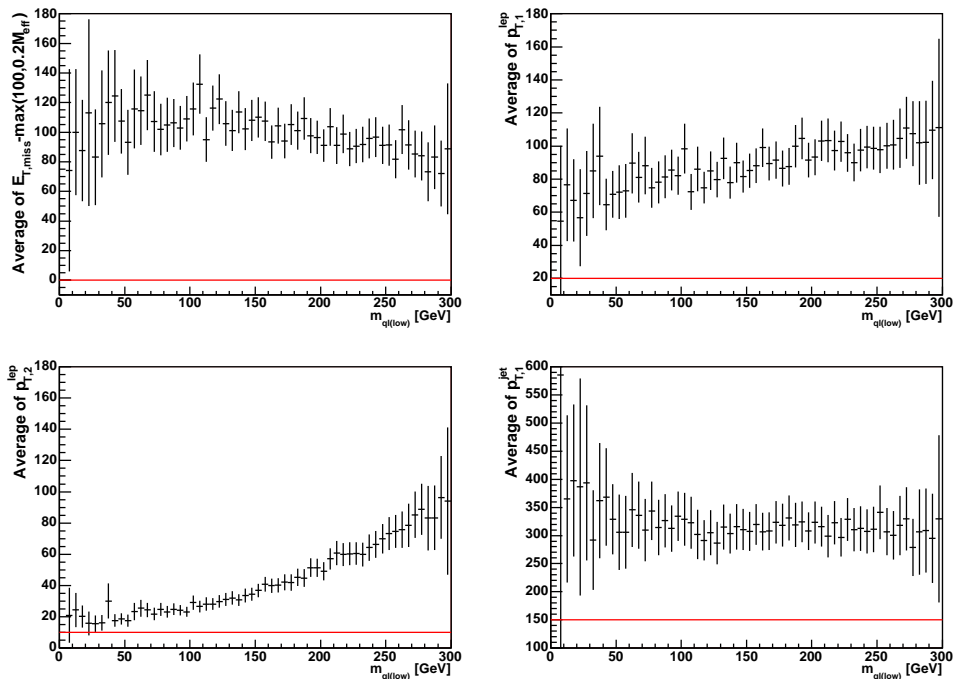


Figure 7: Average value of the cut variables $E_{T,\text{miss}} - \max(100, 0.2M_{\text{eff}})$, $p_{T,1}^{\text{lep}}$, $p_{T,2}^{\text{lep}}$ and $p_{T,1}^{\text{jet}}$, versus invariant mass for $m_{ql(\text{low})}$ (black). We impose the cuts described in the text on the invariant mass distribution before computing averages, but include no FSR. The horizontal lines (red) show the cuts described in the text.

SUSY masses, but that the precision will be limited by that of the jet energy scale.

4. Detector effects

In section 3 we showed that the shape of the invariant mass distributions from the decay chain in eq. (1.1) to a large extent survived parton level effects and cuts to remove SM background. We demonstrated a method of showing whether and where cuts could deform the distribution, making our shape predictions from the kinematics of the decay chain unreliable. What remains to be discussed are the effects of the detector in a given experiment and the combinatorial complications introduced by trying to pick jets that correspond to the quarks in the decay chain.

For this purpose we use AcerDET 1.0 [24], a generic fast detector simulation for the LHC, similar in structure to the ATLFast [25] MC simulation of the ATLAS detector. AcerDET expresses identification and isolation of leptons and jets in terms of detector coordinates by azimuthal angle ϕ , pseudo-rapidity η and cone size $\Delta R = \sqrt{(\Delta\phi)^2 + (\Delta\eta)^2}$. We identify a lepton if $p_T > 5(6)$ GeV and $|\eta| < 2.5$ for electrons (muons). A lepton is isolated if it is a distance $R > 0.4$ from other leptons and jets and the transverse energy deposited in a cone $\Delta R = 0.2$ around the lepton is less than 10 GeV. Jets are reconstructed by a cone-based algorithm from clusters and are accepted if the jet has $p_T > 15$ GeV in

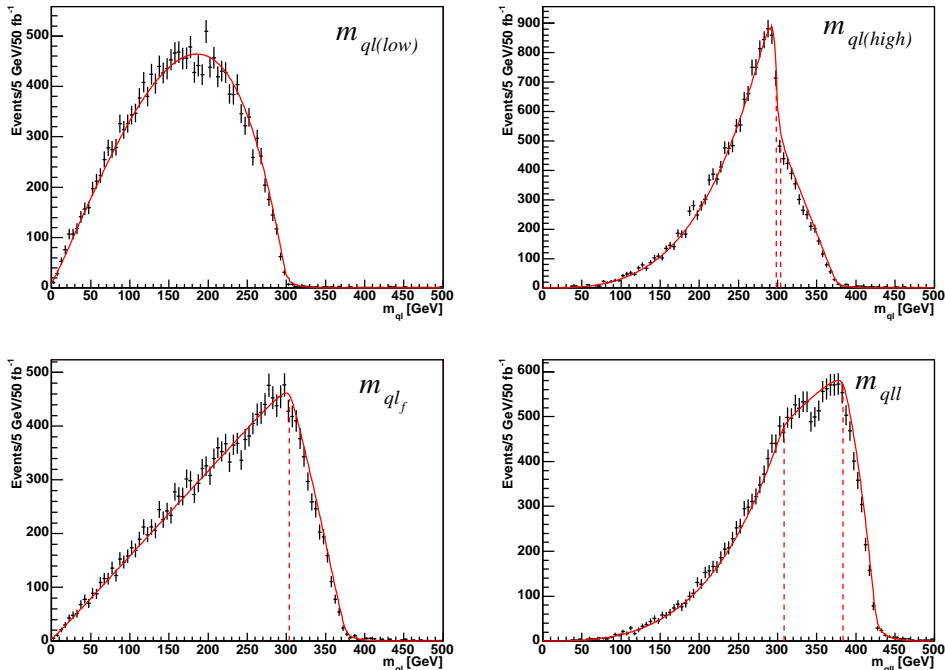


Figure 8: Invariant mass distributions at parton level with FSR included, but no cuts. MC events are shown with errors (black). The lines (red) are the analytic expression with nominal masses. The dashed lines show the ranges of validity of the different function pieces.

a cone $\Delta R = 0.4$. The jets are recalibrated using a flavour independent parametrization, optimized to give a proper scale for the dijet decay of a light (100 GeV) Higgs particle.

As in the parton level discussion we use the mSUGRA model point SPS 1a, a number of events equivalent to 50 fb^{-1} of integrated luminosity generated by PYTHIA 6.208 [17], and the cuts of subsect. 3.2. In addition to the cuts introduced earlier we also cut on b -tagged jets to remove events with a b -squark in the decay chain, which will, due to a smaller squark mass, have a different distribution. We assume 50% b -tagging efficiency with rejection factors 100 and 10 on jets from gluons/three lightest jets and c -jets respectively. While this is on the conservative side it removes a majority of events with b -squarks in the decay chain. However some events remain that will subtly change the distribution. How large a problem this will be will depend on the rate of \tilde{b} production and the efficiency achieved for b -tagging. We have the same issue for the u and d -squarks, since they in general have different masses, but here we cannot tag the jets. One possible solution to this problem is to fit the experimental distributions with the weighted sum of two functions with different squark mass values. This effect is of course smaller than for the b -squark, as the mass difference of these squarks is relatively small in our scenario.

Even if we could remove effectively all events with b -jets another potentially large problem remains. We have no sure way of knowing which jet corresponds to the quark in our decay chain. Since the other jets can stem from the decay of the other SUSY particle produced in the hard process or from the underlying event we cannot rely on “high-low”

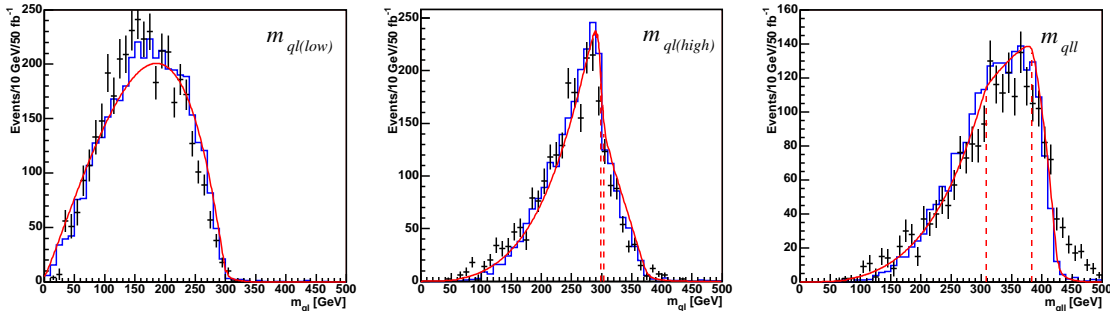


Figure 9: Invariant mass distributions after detector effects and consistency cuts shown with error bars (black). Also shown, are the parton level distributions (blue histograms) with the same normalization as the detector signal and the nominal shapes of the distributions (red curves).

distributions as is done with the two leptons. We therefore propose to use consistency cuts, as discussed in [12], to purify the events. We assume that the endpoints of the distributions have already been estimated, but not necessarily very precisely. To plot the distribution of a given invariant mass among the set: $m_{ql(\text{low})}$, $m_{ql(\text{high})}$ and m_{qll} , we then cut away all events except those where one and only one of the two hardest jets, when combined with the leptons, gives invariant masses that lie below both of the endpoints of the distributions we are not plotting, i.e. that the jet we pick for an event in a given distribution is consistent with the other distributions and that there is no other such consistent jet, among the two hardest ones. Additionally we require that the two leptons have an invariant mass below the endpoint of the m_{ll} distribution. As we shall see, these consistency cuts are very effective in leaving only events where we have picked the right jet to go with the leptons. However they will reduce the number of accepted events significantly, and thus increase statistical errors.

The distributions of the invariant masses $m_{ql(\text{low})}$, $m_{ql(\text{high})}$ and m_{qll} , after detector simulation, after the cuts of section 3.2 and after cuts on b -tagged jets and consistency cuts, are shown in figure 9 with error bars (black). For the consistency cuts we have used as endpoint values $m_{ql(\text{low})}^{\text{max}} = 320$ GeV, $m_{ql(\text{high})}^{\text{max}} = 395$ GeV and $m_{qll}^{\text{max}} = 450$ GeV.⁴ These lie ~ 20 GeV above the fit values of [12], and are clearly well outside the level of uncertainty expected for the measurement of the endpoints, showing that the consistency cuts will not critically depend on measuring the endpoints very accurately. Also in figure 9 (blue histograms) we show the parton level distributions after cuts, rescaled to the reduced number of events in the detector level distributions. Finally, we show the nominal distributions, as given from our formulae (red curves).

From figure 9 we see that the distributions for $m_{ql(\text{low})}$, $m_{ql(\text{high})}$ and m_{qll} in general remain unchanged after detector effects, but compared to figure 8 we have fewer events and thus larger errors. In the $m_{ql(\text{high})}$ distribution we see a rounding of the peak due to additional smearing from energy measurements in the detector simulation. All three

⁴For m_{ll}^{max} we use 80 GeV which is ~ 3 GeV above the fit value.

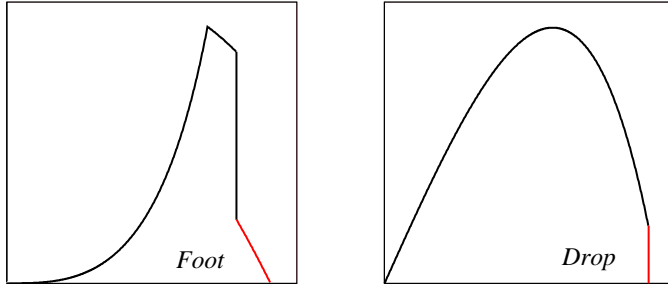


Figure 10: Example of a “foot” and a “drop”.

distributions are also shifted slightly to the left (lower invariant masses) of the nominal shape as a result of imperfect jet recalibration. For the m_{qll} distribution we note that some events with an erroneously picked jet remain to the right of the nominal endpoint of the distribution. The number of these events can be reduced by tighter consistency cuts. Knowing the expected shape of the signal distribution, one could also model the shape of the background and subtract it.

5. Feet

As discussed in [12], the mass values may be such that some invariant mass distributions exhibit “feet” or “drops” at the high ends. These can be hidden by a significant presence of background, taken to be smearing from detector effects or even assumed to be a width effect of the sparticles, making a precise determination of the kinematic maximum, and through these the SUSY masses, difficult and subject to systematic errors.

There are two basic features in the distributions that can result in feet: The first is that the last function piece has a maximum value that is much lower than the global maximum, and so is not taken to be part of the distribution. This we will refer to as a “foot”. The second feature comes about when the last function piece does not fall gradually to zero, but ends in a discontinuous jump. This we will call a “drop”. The two situations are illustrated in figure 10. We will often refer collectively to “feet” and “drops” simply as “feet”.

For both cases, a low value of the ratio between the maximum of the last function piece or the height of the drop, and the global maximum of the distribution will indicate the possible danger of mismeasurements due to feet. We denote this ratio r :

$$r = \frac{\text{height of “foot” or “drop”}}{\text{global maximum}}. \quad (5.1)$$

Without reference to a specific model and thus the size of the background compared to the signal, one can not give an exact value of r where this danger is real, but what can be done is to perform a model independent exploration of what relationships between mass parameters give low ratios.

We will here discuss this for the invariant masses $m_{c2(\text{high})}$, $m_{c2(\text{low})}$ and m_{cba} , in terms of the mass-squared ratios R_A , R_B and R_C introduced in (2.34). With experimental data

one could then use knowledge of the signal to background ratio, with measured values of the mass-squared ratios⁵, to look for such mismeasurements. Finally we will look at the situation for these invariant masses in the $m_{1/2}$ - m_0 -parameter planes around the Snowmass mSUGRA benchmark points SPS1a, SPS1b, SPS3 and SPS5 [14].

5.1 $m_{c2(\text{high})}$

We start our discussion of feet in the different mass distributions by an overview of the *number* of function pieces involved in each region. For the two-particle masses $m_{c2(\text{high})}$ and $m_{c2(\text{low})}$, these are given in table 1.

For the $m_{c2(\text{high})}$ distribution the m_D mass can be factored out of all the function pieces for any value of $m_{c2(\text{high})}$. Taking the ratio of two function pieces, these factors cancel, making the ratio independent of R_C .

Distribution	Region 1	Region 2	Region 3
$m_{c2(\text{high})}$	3	3	3
$m_{c2(\text{low})}$	1	2	2

Table 1: Number of distinct functions for two-particle masses.

For the first two regions we can then

look for a possible foot by finding the ratio r of the maximum of the last function piece to the global maximum in terms of R_A and R_B . The third function piece of the third region does not end at zero, thus it may have a dangerous drop, as described above. The ratio r of the function value at the endpoint to the global maximum can likewise be given in terms of only R_A and R_B . The r -values of all three regions are plotted in figure 11. The results largely agree with those obtained for a particular set of mSUGRA model points in sec. 4.1 of [12], where the shape⁵ of the distribution was generated by a Monte Carlo decay routine.

We find that for Region 1 the ratio is large for most values of R_A and R_B , so that the danger of a foot is small, unless we have a large background to signal ratio. On the other hand, in Region 2, there are large areas with a small value of r where we can have foot effects. One can show that, as a function of R_A and R_B , r is for $m_{c2(\text{high})}$ continuous over the boundary between Regions 1 and 2. Approaching the border to Region 3 the ratio goes to zero. In Region 3, r again takes on large values, even more so than for Region 1. A minimum around $r \simeq 0.60$ excludes the drop scenario from being a danger in this region.

5.2 $m_{c2(\text{low})}$

For the $m_{c2(\text{low})}$ distribution we can also factor out m_D in all regions, with the same factor for all function pieces, so that r again is independent of m_D . In Region 1 the only function piece does not end at zero, and we may thus encounter the drop situation. In Regions 2 and 3 we have a potential foot from the second function piece. In figure 11, we plot the ratio r of eq. (5.1).

In Region 1 we find a strip along the border to Region 2 where we can have a dangerous drop in the distribution. Indeed SPS 1a lies in this region, which is somewhat surprising given that this feature was not noticed in [12]. This clearly shows the advantage of having analytical expressions for the shapes of the distributions. However, the drop here is so small, $r \approx 0.046$, that the resulting mismeasurement of the endpoint amounts to 0.1%, much less than the statistical error. For Regions 2 and 3 r is again continuous over the

⁵The ratios R_A , R_B and R_C can to some extent be determined from the shapes of the distributions alone, and are thus not so susceptible to the effects of a mismeasurement of an endpoint.

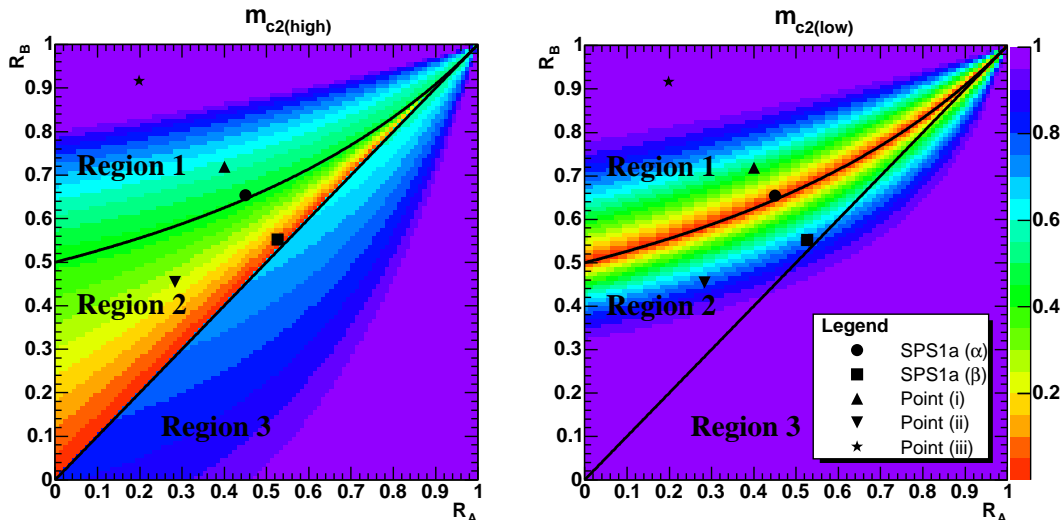


Figure 11: Contour lines of r for all three regions of the $m_{c2(\text{high})}$ (left) and $m_{c2(\text{low})}$ (right) distributions, plotted in the $R_A R_B$ -plane. We also show the position of the points SPS 1a (α), SPS 1a (β), (i), (ii) and (iii), referred to in the discussion of “feet” in [12].

border. The potential for a foot is however restricted to a small strip along the border to Region 1.

5.3 m_{cba}

The numbers of function pieces found in each region and subregion of the three-particle mass distribution are shown in table 2.

In the three-particle case we can no longer remove R_C from the discussion of feet. However, other simplifications arise. One can show that none of the four regions of the m_{cba} distribution has a drop as the last function piece goes to zero at the kinematical endpoint for all regions and subregions. What remains is the possibility of a foot. In figure 12, the ratio r is shown for two values of R_C .

Region	Subreg. 1	Subreg. 2	Subreg. 3
1	3	3	
2	3	3	
3	3		
4	4	4	4

Table 2: Number of distinct functions for the three-particle mass m_{cba} .

In the entirety of Regions 1, 2 and 3 we have $r = 1$ with no danger of feet because the global maximum is in the last function piece. Only in Region 4 can a foot occur. The dangerous regions are near the border between Region 4 and either Region 1 or Region 2, which have low values of r and potentially a misleading foot. Comparing the plots for $R_C = \frac{1}{3}$ and $R_C = \frac{1}{2}$ we see how the value of r changes with R_C inside Region 4, and in particular observe that the points where Regions 1 and 2 meet and where Regions 1 and 3 meet also depend on R_C . However, for m_{cba} , the final function piece often has a steep negative slope after the maximum, which reduces the possible negative effect of a foot.

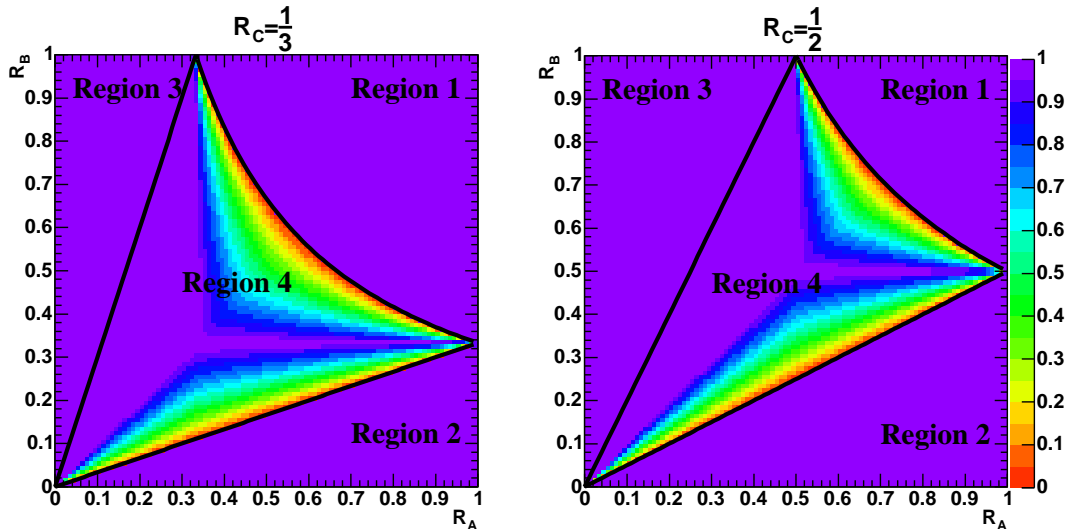


Figure 12: Value of r in all four regions of the m_{cba} distribution, plotted in the $R_A R_B$ -plane for $R_C = \frac{1}{3}$ (left) and $R_C = \frac{1}{2}$ (right).

5.4 SPS benchmark points

In figures 13 and 14 we show the value of r in the $m_{1/2}$ - m_0 -planes around the Snowmass mSUGRA points SPS1a, SPS1b, SPS3 and SPS5, for the $m_{c2(\text{high})}$ and $m_{c2(\text{low})}$ distributions respectively. In the top left panel we have $\tan \beta = 10$ and $A_0 = -m_0$ and in the upper right panel, $\tan \beta = 30$ and $A_0 = 0$. The lower left panel has $\tan \beta = 10$ and $A_0 = 0$ and the lower right panel, $\tan \beta = 5$ and $A_0 = -1000$ GeV. We have only considered parameter values where we have decay chains of the type given in eq. (1.1), with an on-shell, right-handed slepton. For the analogous decay chain via left-handed sleptons, there is no danger of feet for values of $m_{1/2}$ up to 1 TeV. In the gray area we have $m_{\tilde{\chi}_2^0} < m_{\tilde{l}_R}$, thus the decay is only possible via a virtual slepton. The white area, marked TF, is theoretically forbidden and the light brown area has a charged LSP.

In the mSUGRA planes we see that the dangerous area for the $m_{c2(\text{high})}$ distribution lies in the narrow Region 2, and for the $m_{c2(\text{low})}$ distribution in a fairly narrow corridor along the border between Regions 1 and 2. The WMAP-consistent bulk region at low $m_{1/2}$ and m_0 in the top left panels of figures 13 and 14, around the point SPS1a, lies in these dangerous areas. This can be compared to the SPS3 parameter line running along the WMAP-consistent stau coannihilation region in the bottom left panel, and we see that there is little risk of problems with feet in the stau coannihilation region for values of $m_{1/2}$ that are still viable when we consider LEP limits on SUSY masses and on the lightest Higgs. However, this conclusion is only valid for relatively low values of $\tan \beta$. In the top right panel we have $\tan \beta = 30$, and indeed the dangerous area crosses the stau coannihilation region running along the border to the region with a stau LSP. The lower right panel shows that the WMAP-consistent stop coannihilation region, to the left of SPS5, along the theoretically forbidden region, is also dangerous in this respect.

We do not show results for m_{cba} in these parameter planes as we find only points in

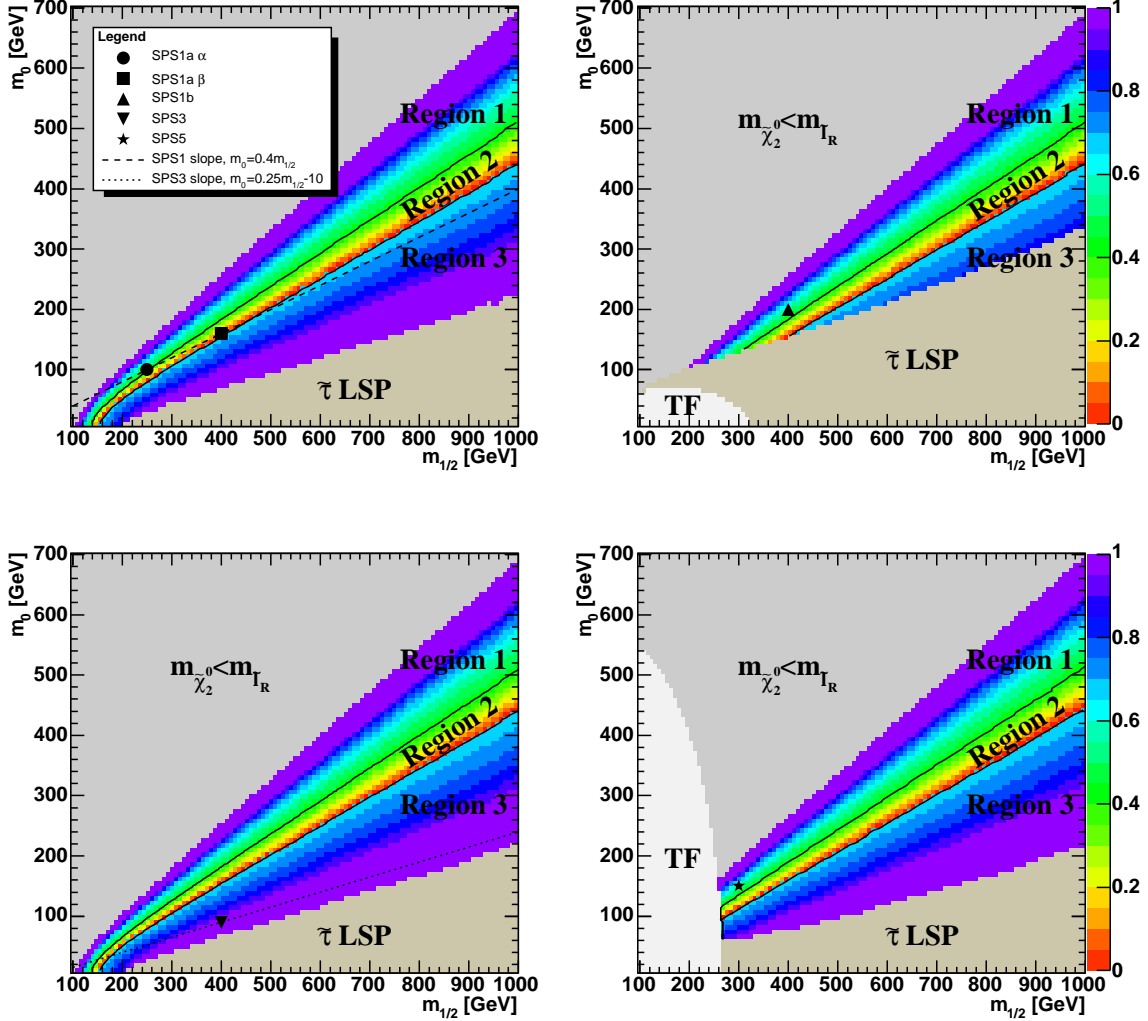


Figure 13: Value of r for the $m_{c2(\text{high})}$ invariant mass distribution in the $m_{1/2}$ - m_0 -planes around the Snowmass benchmark points SPS1a, SPS1b, SPS3 and SPS5.

Region 1 of the m_{cba} distribution in the mSUGRA planes we consider here, for values of $m_{1/2} < 3$ TeV. As discussed above, Region 1 in this distribution contains no dangerous “feet”.

6. Summary

We have derived analytical expressions for the invariant mass distributions of massless SM endproducts c , b , a , in cascade decays of the form $D \rightarrow Cc \rightarrow Bbc \rightarrow Aabc$. Our main results are valid for the decays of spin-0 particles, D , C , B , or equivalently, for a sum over all combinations of charge and chirality in the final states. In a hadron collider environment, the difficulty of determining the charge of quarks from the jets they instigate,

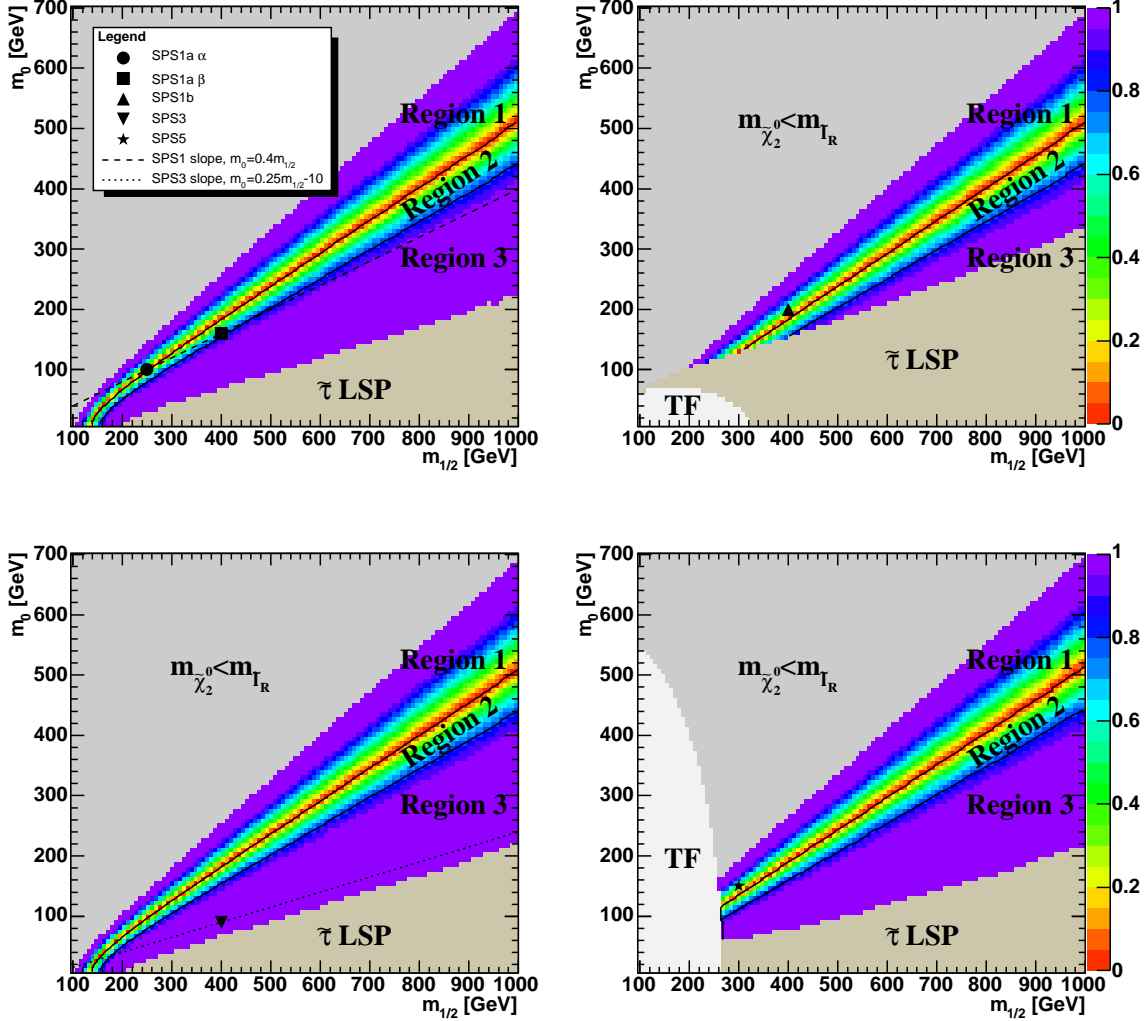


Figure 14: Value of r for the $m_{c2(\text{low})}$ invariant mass distribution in the $m_{1/2}$ - m_0 -planes around the Snowmass benchmark points SPS1a, SPS1b, SPS3 and SPS5.

makes this a reasonable simplification. We have discussed how different spin configurations can easily be included in the distributions, and in the appendix show the corresponding distributions for the specific SUSY decay chain given in (1.1).

The effects of cuts, particle widths and final state radiation on the shape of the distributions have been investigated with PYTHIA in a particular SUSY scenario, the Snowmass benchmark point SPS1a. We find that while a set of cuts used to remove SM background have the potential of distorting the expected shape we can identify which cuts are responsible for this, and in which regions of invariant mass this distortion takes place, by looking at the distribution of the cut parameters, and without resorting to Monte Carlo truth information. The effect of particle widths can be compensated for by a parametrized

smearing of the distribution. Final state radiation introduces a systematic loss of energy, thus shifting the invariant mass distributions towards lower values.

We have also studied the effects of a generic LHC detector, in the same SUSY model, through the use of the fast detector simulation AcerDET. The analytic expressions for the invariant mass distributions is seen to survive the smearing effects of the detector, and we demonstrate a method for handling the combinatorial problem of picking the correct jet that belongs to the decay under investigation, from amongst the many candidates. This consistency cut method is shown to be very effective in removing combinatorial background, but results in a significant reduction in the number of events. The question of whether it is optimal to use cuts to reduce this background, or whether to try to model and subtract it, is still open. A small, systematic shift of the distributions towards lower invariant masses is observed. This indicates that the reconstruction of jets and the jet recalibration routine in the detector simulation, is insufficient for jets from this decay chain, and imply the unsurprising conclusion that understanding the jet energy scale will be essential in reducing systematical uncertainties in parameter determination from the shapes of the invariant mass distributions.

We also demonstrate an application of the analytical expressions in finding dangerous “feet” in the distributions, that could lead to mismeasurements of distribution endpoints, and in turn masses. In scans over mSUGRA parameter space we find that this danger exists for several WMAP-consistent regions: the bulk region and the stau- and stop-coannihilation regions.

Acknowledgments

This research has been supported in part by the Research Council of Norway, and the UK Particle Physics and Astronomy Research Council. PO and ARR thank the CERN Theory Group for hospitality while part of this work was done.

A. Including spin in a SUSY scenario

One can add spin effects in the decay chain by multiplying the integrand with a suitable angular dependent function $f_u(u)$ or $f_v(v)$, depending on the spin configuration in question. We will here give the results of including spin in the SUSY decay chain (1.1), as discussed in the Introduction. In this decay chain we have $A = \tilde{\chi}_1^0$, $B = \tilde{l}$, $C = \tilde{\chi}_2^0$ and $D = \tilde{q}_L$. The spin- $\frac{1}{2}$ of $\tilde{\chi}_2^0$ will yield an extra factor of either $2u$ or $2(1 - u)$ depending on the different combinations of chirality and charge in the final state for the quark and the “near” lepton, as given in table 3. Only the decays starting from a left handed squark are listed fully, those for the right handed squark follow from a simple interchange of left and right handedness⁶. The “far” lepton does not contribute any spin-dependent factor, since the LSP, associated with that fermion line, is not observed.

⁶Note that the handedness of sparticles refer to the chirality of the SM particles they couple to.

Process	chirality of q	chirality of l_n	chirality of l_f	Factor
$\tilde{q}_L \rightarrow ql_n^- l_f^+ \tilde{\chi}_1^0$	L	L	L	$2u$
$\tilde{q}_L \rightarrow ql_n^+ l_f^- \tilde{\chi}_1^0$	L	L	L	$2(1-u)$
$\tilde{\tilde{q}}_L \rightarrow \bar{q}l_n^+ l_f^- \tilde{\chi}_1^0$	L	L	L	$2u$
$\tilde{\tilde{q}}_L \rightarrow \bar{q}l_n^- l_f^+ \tilde{\chi}_1^0$	L	L	L	$2(1-u)$
$\tilde{q}_L \rightarrow ql_n^- l_f^+ \tilde{\chi}_1^0$	L	R	R	$2(1-u)$
$\tilde{q}_L \rightarrow ql_n^+ l_f^- \tilde{\chi}_1^0$	L	R	R	$2u$
$\tilde{\tilde{q}}_L \rightarrow \bar{q}l_n^+ l_f^- \tilde{\chi}_1^0$	L	R	R	$2(1-u)$
$\tilde{\tilde{q}}_L \rightarrow \bar{q}l_n^- l_f^+ \tilde{\chi}_1^0$	L	R	R	$2u$
$\tilde{q}_R \rightarrow ql_n^- l_f^+ \tilde{\chi}_1^0$	R	L	L	$2(1-u)$
\vdots	\vdots	\vdots	\vdots	\vdots
$\tilde{q}_R \rightarrow ql_n^+ l_f^- \tilde{\chi}_1^0$	R	R	R	$2u$
\vdots	\vdots	\vdots	\vdots	\vdots

Table 3: Spin factors. The chirality L/R of l^+ (\bar{q}) denotes that it is the antiparticle of a left-/right-handed l^- (q).

Except for the first case, discussed in section A.1, we shall not give explicit formulas for both chirality cases. The two cases are related as follows:

$$\frac{1}{\Gamma} \frac{\partial \Gamma}{\partial m^2} \Big|_{2(1-u)} = \frac{2}{\Gamma_0} \frac{\partial \Gamma_0}{\partial m^2} - \frac{1}{\Gamma} \frac{\partial \Gamma}{\partial m^2} \Big|_{2u}. \quad (\text{A.1})$$

The integrated decay widths Γ are for both chirality configurations equal to Γ_0 , since the spin correlations only introduce forward-backward asymmetries (in the $\tilde{\chi}_2^0$ rest frame), which integrate to zero.

A.1 m_{ca}

We begin by including spin in the m_{ca} distribution by multiplying the RHS of eq. (2.14) with $f_u(u)$. We find for the $f_u(u) = 2u$ case that

$$\frac{1}{\Gamma} \frac{\partial \Gamma}{\partial m_{ca}^2} = \begin{cases} \frac{2}{(m_{ca}^{\max})^2 a^2} \left[\ln \frac{m_C^2}{m_B^2} - a \right] & \text{for } 0 < m_{ca} < \frac{m_B}{m_C} m_{ca}^{\max}, \\ \frac{2}{(m_{ca}^{\max})^2 a^2} \left[\ln \frac{(m_{ca}^{\max})^2}{m_{ca}^2} + \frac{m_{ca}^2}{(m_{ca}^{\max})^2} - 1 \right] & \text{for } \frac{m_B}{m_C} m_{ca}^{\max} < m_{ca} < m_{ca}^{\max}, \end{cases} \quad (\text{A.2})$$

and for $f_u(u) = 2(1-u)$ we have

$$\frac{1}{\Gamma} \frac{\partial \Gamma}{\partial m_{ca}^2} = \begin{cases} \frac{2}{(m_{ca}^{\max})^2 a^2} \left[\frac{m_B^2}{m_C^2} \ln \frac{m_B^2}{m_C^2} + a \right] & \text{for } 0 < m_{ca} < \frac{m_B}{m_C} m_{ca}^{\max}, \\ \frac{2}{(m_{ca}^{\max})^2 a^2} \left[\frac{m_B^2}{m_C^2} \ln \frac{m_{ca}^2}{(m_{ca}^{\max})^2} - \frac{m_{ca}^2}{(m_{ca}^{\max})^2} + 1 \right] & \text{for } \frac{m_B}{m_C} m_{ca}^{\max} < m_{ca} < m_{ca}^{\max}. \end{cases} \quad (\text{A.3})$$

This confirms the result of [20]. As required, the average of the two again gives eq. (2.20).

A.2 $m_{c2(\text{high})}$

For Region 1 of the $m_{c2(\text{high})}$ distribution, multiplying (2.26) by $f_u(u) = 2u$ gives

$$\frac{1}{\Gamma} \frac{\partial \Gamma}{\partial m_{c2(\text{high})}^2} = \begin{cases} \frac{2}{(m_{ca}^{\max})^2 a^2} \left[\ln \frac{(m_{cb}^{\max})^2}{(m_{cb}^{\max})^2 - am_{c2(\text{high})}^2} - \frac{am_{c2(\text{high})}^2}{(m_{cb}^{\max})^2} \frac{(m_{cb}^{\max})^2 - 2am_{c2(\text{high})}^2}{(m_{cb}^{\max})^2 - am_{c2(\text{high})}^2} \right] \\ \quad \text{for } 0 < m_{c2(\text{high})} < m_{cb}^{\max}, \\ \frac{2}{(m_{ca}^{\max})^2 a^2} \left[\ln \frac{m_C^2}{m_B^2} - a \right] & \text{for } m_{cb}^{\max} < m_{c2(\text{high})} < \frac{m_B}{m_C} m_{ca}^{\max}, \\ \frac{2}{(m_{ca}^{\max})^2 a^2} \left[\ln \frac{(m_{ca}^{\max})^2}{m_{c2(\text{high})}^2} + \frac{m_{c2(\text{high})}^2}{(m_{ca}^{\max})^2} - 1 \right] \\ \quad \text{for } \frac{m_B}{m_C} m_{ca}^{\max} < m_{c2(\text{high})} < m_{ca}^{\max}. \end{cases} \quad (\text{A.4})$$

For Region 2 we get

$$\frac{1}{\Gamma} \frac{\partial \Gamma}{\partial m_{c2(\text{high})}^2} = \begin{cases} \frac{2}{(m_{ca}^{\max})^2 a^2} \left[\ln \frac{(m_{cb}^{\max})^2}{(m_{cb}^{\max})^2 - am_{c2(\text{high})}^2} - \frac{am_{c2(\text{high})}^2}{(m_{cb}^{\max})^2} \frac{(m_{cb}^{\max})^2 - 2am_{c2(\text{high})}^2}{(m_{cb}^{\max})^2 - am_{c2(\text{high})}^2} \right] \\ \quad \text{for } 0 < m_{c2(\text{high})} < m_{c2(\text{eq})}^{\max}, \\ \frac{2}{(m_{ca}^{\max})^2 a^2} \left[\ln \frac{(m_{ca}^{\max})^2}{m_{c2(\text{high})}^2} + \frac{a^2 (m_{ca}^{\max})^2 m_{c2(\text{high})}^2}{(m_{cb}^{\max})^4} + \frac{m_{c2(\text{high})}^2}{(m_{ca}^{\max})^2} - 1 \right] \\ \quad \text{for } m_{c2(\text{eq})}^{\max} < m_{c2(\text{high})} < m_{cb}^{\max}, \\ \frac{2}{(m_{ca}^{\max})^2 a^2} \left[\ln \frac{(m_{ca}^{\max})^2}{m_{c2(\text{high})}^2} + \frac{m_{c2(\text{high})}^2}{(m_{ca}^{\max})^2} - 1 \right] \text{ for } m_{cb}^{\max} < m_{c2(\text{high})} < m_{ca}^{\max}. \end{cases} \quad (\text{A.5})$$

For Region 3 we have

$$\frac{1}{\Gamma} \frac{\partial \Gamma}{\partial m_{c2(\text{high})}^2} = \begin{cases} \frac{2}{(m_{ca}^{\max})^2 a^2} \left[\ln \frac{(m_{cb}^{\max})^2}{(m_{cb}^{\max})^2 - am_{c2(\text{high})}^2} - \frac{am_{c2(\text{high})}^2}{(m_{cb}^{\max})^2} \frac{(m_{cb}^{\max})^2 - 2am_{c2(\text{high})}^2}{(m_{cb}^{\max})^2 - am_{c2(\text{high})}^2} \right] \\ \quad \text{for } 0 < m_{c2(\text{high})} < m_{c2(\text{eq})}^{\max}, \\ \frac{2}{(m_{ca}^{\max})^2 a^2} \left[\ln \frac{(m_{ca}^{\max})^2}{m_{c2(\text{high})}^2} + \frac{a^2 (m_{ca}^{\max})^2 m_{c2(\text{high})}^2}{(m_{cb}^{\max})^4} + \frac{m_{c2(\text{high})}^2}{(m_{ca}^{\max})^2} - 1 \right] \\ \quad \text{for } m_{c2(\text{eq})}^{\max} < m_{c2(\text{high})} < m_{ca}^{\max}, \\ \frac{2m_{c2(\text{high})}^2}{(m_{cb}^{\max})^4} & \text{for } m_{ca}^{\max} < m_{c2(\text{high})} < m_{cb}^{\max}. \end{cases} \quad (\text{A.6})$$

A.3 $m_{c2(\text{low})}$

For the $m_{c2(\text{low})}$ distribution, in Region 1, and with $f_u(u) = 2u$, we get

$$\frac{1}{\Gamma} \frac{\partial \Gamma}{\partial m_{c2(\text{low})}^2} = \frac{2}{(m_{ca}^{\max})^2 a^2} \left[\ln \frac{(m_{cb}^{\max})^2 - am_{c2(\text{low})}^2}{\frac{m_B^2}{m_C^2} (m_{cb}^{\max})^2} + \frac{a^2 m_{c2(\text{low})}^2 (m_{ca}^{\max})^2}{(m_{cb}^{\max})^4} \right. \\ \left. - \frac{a^2 m_{c2(\text{low})}^4}{(m_{cb}^{\max})^2 [(m_{cb}^{\max})^2 - am_{c2(\text{low})}^2]} + \frac{am_{c2(\text{low})}^2}{(m_{cb}^{\max})^2} - a \right], \quad (\text{A.7})$$

for $0 < m_{c2(\text{low})} < m_{cb}^{\max}$. For Regions 2 and 3 the distribution is for $f_u(u) = 2u$ given by

$$\frac{1}{\Gamma} \frac{\partial \Gamma}{\partial m_{c2(\text{low})}^2} = \frac{2}{(m_{ca}^{\max})^2 a^2} \left\{ \begin{array}{l} \ln \frac{(m_{cb}^{\max})^2 - am_{c2(\text{low})}^2}{\frac{m_B^2}{m_C^2} (m_{cb}^{\max})^2} + \frac{a^2 (m_{ca}^{\max})^2 m_{c2(\text{low})}^2}{(m_{cb}^{\max})^4} \\ - \frac{a^2 m_{c2(\text{low})}^4}{(m_{cb}^{\max})^2 [(m_{cb}^{\max})^2 - am_{c2(\text{low})}^2]} + \frac{am_{c2(\text{low})}^2}{(m_{cb}^{\max})^2} - a \\ \text{for } 0 < m_{c2(\text{low})} < \frac{m_B}{m_C} m_{ca}^{\max}, \\ \ln \frac{(m_{ca}^{\max})^2 [(m_{cb}^{\max})^2 - am_{c2(\text{low})}^2]}{(m_{cb}^{\max})^2 m_{c2(\text{low})}^2} + \frac{a^2 (m_{ca}^{\max})^2 m_{c2(\text{low})}^2}{(m_{cb}^{\max})^4} \\ - \frac{a^2 m_{c2(\text{low})}^4}{(m_{cb}^{\max})^2 [(m_{cb}^{\max})^2 - am_{c2(\text{low})}^2]} + \frac{m_{c2(\text{low})}^2}{(m_{ca}^{\max})^2} + \frac{am_{c2(\text{low})}^2}{(m_{cb}^{\max})^2} - 1 \\ \text{for } \frac{m_B}{m_C} m_{ca}^{\max} < m_{c2(\text{low})} < m_{c2(\text{eq})}^{\max}. \end{array} \right. \quad (\text{A.8})$$

A.4 m_{cba}

In the m_{cba} distribution the spin factor enters into the integral $L(a_1, a_2)$ of eq. (2.71). We define a new integral:

$$M(a_1, a_2) \equiv \int_{a_1}^{a_2} \frac{y}{\sqrt{y^2 + 2ym_B + m_B^2 - m_D^2}} dy \\ = \sqrt{y^2 + 2ym_B + m_B^2 - m_D^2} \Big|_{a_1}^{a_2} - m_B L(a_1, a_2). \quad (\text{A.9})$$

For all four Regions of the m_{cba} distribution the effect of the neutralino spin can be added by making the following simple substitution in the distributions of eqs. (2.89)–(2.96), for the $f_u(u) = 2u$ case:

$$L(a_1, a_2) \rightarrow L'(a_1, a_2) = \frac{2(m_D^2 - m_B^2)m_C^2 L(a_1, a_2) - 4m_B m_C^2 M(a_1, a_2)}{(m_D^2 - m_C^2)(m_C^2 - m_B^2)}. \quad (\text{A.10})$$

References

- [1] J. Wess and B. Zumino, Nucl. Phys. B **70**, 39 (1974).
- [2] P. Fayet and S. Ferrara, Phys. Rept. **32** (1977) 249.
- [3] S. Dimopoulos and H. Georgi, Nucl. Phys. B **193** (1981) 150.
- [4] H. P. Nilles, Phys. Rept. **110** (1984) 1.
- [5] H. E. Haber and G. L. Kane, Phys. Rept. **117** (1985) 75.
- [6] I. Hinchliffe, F. E. Paige, M. D. Shapiro, J. Soderqvist and W. Yao, Phys. Rev. D **55** (1997) 5520 [arXiv:hep-ph/9610544].
- [7] I. Hinchliffe, F. E. Paige, E. Nagy, M. D. Shapiro, J. Soderqvist and W. Yao, LBNL-40954
- [8] H. Bachacou, I. Hinchliffe and F. E. Paige, Phys. Rev. D **62** (2000) 015009 [arXiv:hep-ph/9907518].
- [9] G. Polesello, *Precision SUSY measurements with ATLAS for SUGRA point 5*, ATLAS Internal Note, PHYS-No-111, October 1997.
- [10] B. C. Allanach, C. G. Lester, M. A. Parker and B. R. Webber, JHEP **0009** (2000) 004 [arXiv:hep-ph/0007009].
- [11] C. G. Lester, *Model independent sparticle mass measurements at ATLAS*, Ph. D. thesis, <http://www.slac.stanford.edu/spires/find/hep/www?r=cern-thesis-2004-003>
- [12] B. K. Gjelsten, D. J. Miller and P. Osland, JHEP **12** (2004) 003 [arXiv:hep-ph/0410303].
- [13] B. K. Gjelsten, D. J. Miller and P. Osland, JHEP **06** (2005) 015 [arXiv:hep-ph/0501033].
- [14] B. C. Allanach *et al.*, in *Proc. of the APS/DPF/DPB Summer Study on the Future of Particle Physics (Snowmass 2001)* ed. N. Graf, Eur. Phys. J. C **25** (2002) 113 [eConf **C010630** (2001) P125] [arXiv:hep-ph/0202233].
- [15] T. Appelquist, H. C. Cheng and B. A. Dobrescu, Phys. Rev. D **64**, 035002 (2001) [arXiv:hep-ph/0012100].
- [16] H. C. Cheng, K. T. Matchev and M. Schmaltz, Phys. Rev. D **66** (2002) 056006 [arXiv:hep-ph/0205314].
- [17] T. Sjöstrand, P. Edén, C. Friberg, L. Lönnblad, G. Miu, S. Mrenna, E. Norrbin, Comput. Phys. Commun. **135** (2001) 238; T. Sjöstrand, L. Lönnblad and S. Mrenna, “PYTHIA 6.2: Physics and manual”, arXiv:hep-ph/0108264.
- [18] P. Richardson, JHEP **0111** (2001) 029 [arXiv:hep-ph/0110108].
- [19] A. J. Barr, arXiv:hep-ph/0405052.
- [20] J. M. Smillie and B. R. Webber, arXiv:hep-ph/0507170.

- [21] A. Birkedal, R. C. Group and K. Matchev, arXiv:hep-ph/0507002.
- [22] H. Baer, F. E. Paige, S. D. Protopopescu and X. Tata, arXiv:hep-ph/9305342, arXiv:hep-ph/0001086.
- [23] H. L. Lai *et al.* [CTEQ Collaboration], Eur. Phys. J. C **12** (2000) 375 [arXiv:hep-ph/9903282].
- [24] E. Richter-Was, arXiv:hep-ph/0207355.
- [25] E. Richter-Was, D. Froidevaux and L. Poggioli, “ATLFAST 2.0: a fast simulation package for ATLAS”, Tech. Rep. ATL-PHYS-98-131 (1998).